arXiv:2608.20194v1 [physics.chem-ph] 20 Aug 2026

Observables and anti-Hermitian generators in time-dependent unitary coupled cluster theory

Martín A. Mosquera

Department of Chemistry and Biochemistry, Montana State University, Bozeman, Montana 59717, USA

E-mail: martinmosquera@montana.edu

Keywords: unitary coupled cluster, anti-Hermiticity, generator, time-dependence, electronic structure

Abstract

This work presents a time-dependent (TD) unitary coupled-cluster (UCC) formulation for electronic quantum dynamics, including the propagation of excited states and their superpositions, in both single- and multi-reference regimes. Standard TD coupled-cluster techniques offer size-extensivity, but they rely on non-Hermitian bivariational action functionals that break time-reversibility, giving transition matrix elements and amplitude estimators that are asymmetric (though accurate and systematically improvable). Here we use the time-evolution operator as an exponential map driven by TD anti-Hermitian cluster operators and first-order generators. Applying the Dirac-Frenkel action principle, we extract equations of motion governed by Heisenberg-picture-like commutators. This approach connects to our previous non-Hermitian formulations, where observables are expressed in terms of regular and extended cluster operators. From that connection we obtain a generator cluster operator whose unperturbed TD limit leads to the UCC eigenvalue problem. Even though this problem can be exact, the time dependence of the generator holds only at short propagation times, so we use the generator to prepare the initial state and then propagate that state with the formal TD UCC equation of motion. The theory is tested on an extended hard-core Bose-Hubbard ring with connections to neutral atom chains, and we discuss the theory's present limitations and possible extensions.

1 Introduction

The systematically improvable computation of real-time quantum dynamics is essential to understand the behavior of strongly correlated systems driven out of equilibrium. Examples of these phenomena span attosecond photochemistry, non-adiabatic multi-state dynamics, and the coherent control of molecular materials [1–12]. Quantum Information Science (QIS) has matured around controllable hardware platforms such as superconducting circuits, photonic networks, and trapped ions [13–16]. Programmable neutral atom clusters and Rydberg atom arrays are also emerging as platforms for quantum computation and analog many-body quantum simulation [17–37]. These neutral atom systems offer fine spatial control and long coherence times, but putting their multi-reference configurations to practical use relies on a microscopic understanding of their coherent, real-time evolution under external electromagnetic driving forces.

For accurate stationary ground-state simulations, Coupled-Cluster (CC) theory is a standard in *ab initio* quantum chemistry due to its size-extensivity capabilities and elegant treatment of many-body correlation [38–44]. For excited states, frameworks such as the symmetry-adapted-cluster CI [45, 46], Linear Response CC, and Equation-of-Motion CC obtain spectra by diagonalizing the non-Hermitian similarity-transformed Hamiltonian [47–56]. Separately, extensive developments in Multireference CC (MRCC) have enabled accurate targeting of strongly correlated ground and excited states [57–74]. The real-time dynamics of these systems under external time-dependent perturbations is a challenging problem. Standard

Time-Dependent CC (TD-CC) methods rely on the bivariational principle introduced by Arponen, Dalgaard, and Monkhorst [75, 76]. Because the similarity transformation is non-unitary, the bra and ket states must be parameterized as distinct, independent degrees of freedom. This has nonetheless led to powerful approaches and applications [77–97]. Standard TD-CC yields transition matrix elements that break time-reversibility, sacrificing formal Hermitian symmetry [98]. In some cases, restoring this property comes at the expense of losing some other desirable aspect [99, 100].

To avoid these asymmetries and restore physical Hermiticity, one can rely on unitary coupled-cluster (UCC) theory [101–105]. Standard ground-state UCC restricts the cluster operators to be anti-Hermitian; as a consequence, the sum-over-states polarization propagator and transition moments feature the correct symmetric properties [105]. UCC has a long history, including self-consistent electron propagator theory [102, 106] and property calculations without quantum phase estimation [107], but its resurgence is tied to its being a source of *ansatz* for chemistry algorithms formulated for quantum computing [108–123]. For hardware, current circuit depths demand approximations such as nonunitary extensions via midcircuit measurements [124], or quantum variants of the Davidson algorithm for excited states [125]. The outstanding difficulty in UCC is the non-terminating Baker-Campbell-Hausdorff (BCH) expansion and the implied non-commutative algebra. Classical implementations have worked around it with automated non-antisymmetric tensor contractions [126]. The internally contracted EOM (equation-of-motion) UCC formalism effectively truncates the series off at the four-fold commutator level [127]; there the excited states are built from a forward-only excitation operator and obtained as a stationary eigenvalue problem, rather than as the time-dependent superpositions propagated here. Downfolding methods such as the Double Unitary Coupled-Cluster formalism take a different route, partitioning space and orbitals to decouple internal degrees of freedom [128, 129].

Alongside these developments, the author has pursued a sequence of extensions to standard TD-CC aimed at propagating quantum superpositions efficiently while preserving size-extensivity. These are excited-state response theory within the CC framework [130, 131], Second Response Theory [132], and extended Time-Dependent Multireference Coupled-Cluster theory [133]. They treat superpositions as infinitesimal bivariational perturbations, resembling the generators of continuous group theory. The present work investigates the non-commutative approach to the static and time-dependent properties of quantum systems, time-reversibility, and symmetric transition matrix elements in both regimes. The main TD equation for reference propagation follows from the Dirac-Frenkel action and the Maurer-Cartan relations, from which we extract the equation of motion for the generator of excitations. Analyzing its unperturbed dynamics gives the EOM-UCC eigenvalue problem; factoring out unlinked "vacuum" fluctuations leaves a symmetric eigenvalue equation. The solution then provides initial operators that "rotate" the reference, leading to a general equation of motion. Exact numerical simulations of a neutral atom ring model show that the formulation stays well-behaved under mid-to-strong correlation conditions.

2 Theory

2.1 Correlated Ground State

This work concerns propagation under non-relativistic Hamiltonians of the kind $\hat{H}(t) = \hat{H}_0 + \hat{V}(t)$, where $\hat{H}_0$ is the static component and $\hat{V}(t)$ represents an external driving TD potential. The operator $\hat{H}_0$, as free Hamiltonian, is used to obtain the eigen-spectrum of the system.

We denote the reference state as $|0\rangle$, which can be constructed through the solution of a multi- or single-reference model. In previous work [133], we used this state to construct the basis excitation operators, $\{\tau_{\bar{\mu}}\}$, through solution of a SVD problem, followed by a QR factorization so this set of operators is similar to the single-reference formalism. This construction slightly differs from standard orthogonalization in internally contracted MRCC [63], which places the external excitations on a contracted footing, and removes the purely internal excitations, which are replaced by orbital relaxation. The SVD discards null directions from the overlap metric (singular values below a threshold η), while the subsequent QR factorization rotates the reference projection onto a single axis, fixing $\hat{\tau}_0 = \hat{1}$ with $\hat{\tau}_0|0\rangle = |0\rangle$, and yielding $\{|\bar{\mu}\rangle = \hat{\tau}_{\bar{\mu}}|0\rangle\}_{\bar{\mu}\geq 0}$ as an orthonormal set. The multireference system depends on a single orthonormal excitation ladder, which makes the formalism below resemble a single-reference one. However, the basis excitation operators do not commute. For theoretical purposes we assume that $[\hat{\tau}_{\bar{\mu}}, \hat{\tau}_{\bar{\nu}}] \neq 0$ in general, unless the system is single-reference or bosonic as in the numerical application, section 3 (in these cases non-commutativity remains present, but only between excitation operators and their conjugate forms). Throughout this work, the $\hat{\tau}_{\bar{\mu}}$ are excitation operators in the general sense. The formalism below uses only their algebra, their mutual non-commutativity, and the action of their adjoints on the reference, not the statistics of the underlying particles. Therefore the formalism applies to fermionic and bosonic systems. We use it here to study a system of hard-core bosons, Sec. 3.1.

The ground state wavefunction is expressed using the anti-Hermitian operator $\hat{T}$:

$$|\Psi_0\rangle \equiv \exp(\hat{T})|0\rangle \ , \quad \text{with} \quad \hat{T}^\dagger = -\hat{T} \ . \tag{1}$$

Because $\hat{T}$ is anti-Hermitian, the ground state $|\Psi_0\rangle$ is normalized ($\langle\Psi_0|\Psi_0\rangle = 1$). Expectation values evaluated over the reference are denoted as $\langle\hat{O}\rangle = \langle 0|\hat{O}|0\rangle$. For example, we average ground-state observables by evaluating the transformed operators over the reference determinant, $\langle\Psi_0|\hat{O}|\Psi_0\rangle = \langle e^{-\hat{T}}\hat{O}e^{\hat{T}}\rangle \equiv \langle\hat{O}_T\rangle$. As expected, the ground state problem is solved by minimizing the energy function $\mathcal{E}(\hat{T}) = \langle\hat{H}_T\rangle$, leading to the stationary condition for the ground state

$$\langle[\hat{H}_T, \hat{\pi}_T(\hat{\kappa}_\mu)]\rangle = 0 \tag{2}$$

for all anti-Hermitian excitation basis operators $\hat{\kappa}_\mu$ (defined next, section 2.2), which lets us write $\hat{T} = \sum_\mu t_\mu \hat{\kappa}_\mu$. The superoperator $\hat{\pi}_T$ is expressed as

$$\hat{\pi}_T \cdot = 1 - \frac{1}{2}[\hat{T}, \cdot] + \frac{1}{3!}[\hat{T}, [\hat{T}, \cdot]] - \cdots = \sum_{n=0}^{\infty} \frac{(-1)^n}{(n+1)!} \mathrm{ad}_{\hat{T}}^n \cdot \ , \tag{3}$$

where the adjoint operation is $\mathrm{ad}_{\hat{T}} \cdot = [\hat{T}, \cdot]$.

2.2 Ground State Propagation

We write the time-evolution operator as $\hat{U}_{\rm m}(t)$, acting on $|0\rangle$ using an anti-Hermitian cluster operator:

$$\hat{U}_{\rm m}(t;g)|0\rangle = \exp\left[\hat{x}_{\rm m}(t;g)\right]|0\rangle \ . \tag{4}$$

The propagation operator $\hat{x}_{\rm m}$ depends on both time and an auxiliary parameter g, which is related to continuous generators (section 2.3). To track real-time transitions, we define an anti-Hermitian basis. We introduce an extended index $\mu \equiv (\bar{\mu}, \sigma)$ that combines the conventional excitation index $\bar{\mu}$ and a type index $\sigma \in \{-, +\}$. The corresponding anti-Hermitian basis operators are defined as:

$$\hat{\kappa}_\mu = \begin{cases} \hat{\tau}_{\bar{\mu}} - \hat{\tau}_{\bar{\mu}}^\dagger & \text{for } \sigma = - \quad \text{(Real antisymmetric)} \\ \mathrm{i}(\hat{\tau}_{\bar{\mu}} + \hat{\tau}_{\bar{\mu}}^\dagger) & \text{for } \sigma = + \quad \text{(Imaginary symmetric)} \end{cases} \tag{5}$$

Conventional CC restricts basis expansions to excitation operators ($\hat{\tau}_{\bar{\mu}}$). Each $\hat{\kappa}_\mu$ above is anti-Hermitian by construction. The real-antisymmetric and imaginary-symmetric sectors let the generator span the full excitation space while preserving the anti-Hermiticity.

The cluster operator $\hat{x}_{\rm m}(t;g)$ is constructed as a single linear expansion over this extended non-scalar index:

$$\hat{x}_{\rm m}(t;g)|0\rangle = \sum_\mu x_{{\rm m},\mu}(t;g)\hat{\kappa}_\mu|0\rangle \ . \tag{6}$$

$x_{{\rm m},\mu}(t;g)$ is the amplitude associated to the $\hat{\kappa}_\mu$ basis state. The basis operators in the expanded set are anti-Hermitian ($\hat{\kappa}_\mu^\dagger = -\hat{\kappa}_\mu$), the generator itself remains anti-Hermitian at all times ($\hat{x}_{\rm m}^\dagger = -\hat{x}_{\rm m}$), ensuring that $\hat{U}_{\rm m}^\dagger(t)\hat{U}_{\rm m}(t) = \mathbf{1}$.

To find the equations of motion, we evaluate the Dirac-Frenkel action over the reference state $|0\rangle$:

$$\mathcal{S} = \int \mathrm{d}t \ \langle \hat{U}_{\rm m}^\dagger(t)[\mathrm{i}\partial_t - \hat{H}(t)]\hat{U}_{\rm m}(t)\rangle \ . \tag{7}$$

The dynamics are determined by the condition $\delta\mathcal{S} = 0$. Since $\hat{U}_{\rm m}(t)$ is unitary, the wave-function is normalized in a robust way. Using differentiation rules for exponential matrices on the state $|\Psi(t)\rangle = \hat{U}_{\rm m}(t)|0\rangle$, we obtain

$$\hat{U}_{\rm m}^\dagger \mathrm{i}\partial_t \hat{U}_{\rm m} = \mathrm{i}\hat{\pi}_{x_{\rm m}}(\partial_t \hat{x}_{\rm m}(t)) \ , \tag{8}$$

where the projection superoperator evaluates to the infinite nested operator commutator expansion:

$$\hat{\pi}_{x_{\rm m}}(\partial_t \hat{x}_{\rm m}(t)) = \sum_{n=0}^{\infty} \frac{(-1)^n}{(n+1)!} \mathrm{ad}_{\hat{x}_{\rm m}(t)}^n \left(\partial_t \hat{x}_{\rm m}(t)\right) \ , \tag{9}$$

we have that $\mathrm{ad}_{\hat{x}_{\rm m}(t)}\hat{O} = [\hat{x}_{\rm m}(t), \hat{O}]$. We used this type of expansion above in previous non-Hermitian work [133]. Now, let us define the fully transformed Hamiltonian $\hat{H}_{x_{\rm m}}(t) = \exp[-\hat{x}_{\rm m}(t)]\hat{H}(t)\exp[\hat{x}_{\rm m}(t)]$, and the residual operator:

$$\hat{R}_{\rm m}(t;g) = \mathrm{i}\hat{\pi}_{x_{\rm m}}(\partial_t \hat{x}_{\rm m}(t;g)) - \hat{H}_{x_{\rm m}}(t;g) \ . \tag{10}$$

Variations of the action over $\hat{x}_{\rm m}$ are taken along the transformed basis directions $\hat{\Xi}_{{\rm m},\mu}(t;g) \equiv \hat{\pi}_{x_{\rm m}}(\hat{\kappa}_\mu)$, i.e., the projection superoperator of Eq. (9) applied to the basis operators $\hat{\kappa}_\mu$ of Eq. (5). This leads to the equations of motion:

$$\langle \left[\hat{\Xi}_{{\rm m},\mu}(t;g) \, , \, \hat{R}_{\rm m}(t;g)\right]\rangle = 0 \ . \tag{11}$$

For $g = 0$ the above gives the equation that propagates the ground state.

2.3 Generators of Excitations

As in our previous formulations, we examine a generator of excitations/de-excitations. We expand $\hat{x}_{\rm m}(t)$ with respect to a continuous parameter g:

$$\hat{x}_{\rm m}(t;g) = \hat{x}(t) + g\hat{z}(t) + \mathcal{O}(g^2) \ . \tag{12}$$

The operator $\hat{x}(t)$ describes the non-linear propagation of the ground state $|\Psi_0\rangle$ under the external field (or $\hat{V}(t)$), while $\hat{z}(t)$ denotes the first-order generator. The initial condition for $\hat{x}(t)$ is:

$$\hat{x}(0) = \hat{T} \ . \tag{13}$$

A weak driving field can lead the system to build such a contribution from an anti-Hermitian operator, giving the generator ($\hat{z}$) a physical origin.

For $g = 0$ the residual reads $\hat{R}_x(t) = \mathrm{i}\hat{\pi}_x(\partial_t\hat{x}(t)) - \hat{H}_x(t)$, where $\hat{H}_x(t)$ is $\exp[-\hat{x}(t)]\hat{H}(t)\exp[\hat{x}(t)]$. Before we extract the EOM for the generator, we differentiate the residual $\hat{R}_{\rm m}$ with respect to g, and define the continuous generator $\tilde{z}(t;g) = \hat{\pi}_{x_{\rm m}}(\partial_g\hat{x}_{\rm m}(t;g))$, the projected form of the first-order generator $\hat{z}(t)$ of Eq. (12). Evaluating this at $g = 0$ leads to the additional definition $\tilde{z}(t) = \tilde{z}(t;g)\big|_{g=0}$.

Now we invoke the Maurer-Cartan (MC) relation (detailed in SI):

$$\partial_g\left(\hat{\pi}_{x_{\rm m}}(\partial_t\hat{x}_{\rm m})\right) = \partial_t\tilde{z}(t;g) + \left[\hat{\pi}_{x_{\rm m}}(\partial_t\hat{x}_{\rm m})\,,\,\tilde{z}(t;g)\right] \ . \tag{14}$$

The g-derivative of the residual thus reads:

$$\partial_g\hat{R}_{\rm m}(t;g) = \mathrm{i}\partial_t\tilde{z}(t;g) + [\hat{R}_{\rm m}(t;g), \tilde{z}(t;g)] \ . \tag{15}$$

Evaluating at $g = 0$, where $\hat{R}_{\rm m}\big|_{g=0} = \hat{R}_x(t)$, yields the term:

$$\hat{R}^{(1)}(t) = \mathrm{i}\partial_t\tilde{z}(t) + [\hat{R}_x(t), \tilde{z}(t)] \ . \tag{16}$$

The basis variations $\hat{\Xi}^{(n)}_\mu(t) = \partial^n_g\hat{\Xi}_{{\rm m},\mu}(t;g)\big|_{g=0}$ are extracted via their respective Lie derivatives (e.g., $\partial_g\hat{\Xi}_{{\rm m},\mu} = \partial_\mu\tilde{z}(t;g) + [\hat{\Xi}_{{\rm m},\mu}, \tilde{z}(t;g)]$, with $\partial_\mu \equiv \partial/\partial x_{{\rm m},\mu}$), giving:

$$\hat{\Xi}^{(0)}_\mu(t) = \hat{\pi}_x(\hat{\kappa}_\mu) \ , \tag{17}$$

$$\hat{\Xi}^{(1)}_\mu(t) = \partial_\mu\tilde{z}(t) + [\hat{\Xi}^{(0)}_\mu(t), \tilde{z}(t)] \ . \tag{18}$$

These are the elements needed to write the dynamical equations for $\tilde{z}(t)$.

The EOM for the ground-state trajectory ($g = 0$) requires the term $\hat{\Xi}^{(0)}_\mu(t)$, and the relation $\langle\left[\hat{\Xi}^{(0)}_\mu(t)\,,\,\hat{R}_x(t)\right]\rangle = 0$. Differentiating Eq. (11) with respect to g and evaluating at $g = 0$ gives the constraint:

$$\langle\left[\hat{\Xi}^{(1)}_\mu(t)\,,\,\hat{R}_x(t)\right]\rangle + \langle\left[\hat{\Xi}^{(0)}_\mu(t)\,,\,\hat{R}^{(1)}(t)\right]\rangle = 0 \ . \tag{19}$$

Substituting the evaluation for the first-order residual $\hat{R}^{(1)}(t)$ into this constraint provides the initial-value equation, where the first-order TD equation for the generator becomes:

$$\langle\left[\hat{\Xi}^{(0)}_\mu(t)\,,\,\mathrm{i}\partial_t\tilde{z}(t)\right]\rangle = -\langle\left[\hat{\Xi}^{(0)}_\mu(t)\,,\,[\hat{R}_x(t), \tilde{z}(t)]\right]\rangle - \langle\left[\hat{\Xi}^{(1)}_\mu(t)\,,\,\hat{R}_x(t)\right]\rangle \ . \tag{20}$$

As shown later on, this relation applies to free and driven propagations, and is accurate at early times.

2.4 Unperturbed Non-Stationary States, Initial Conditions, and Eigenvalue Problem
Propagating a general initial state requires cluster operators at $t = 0$. We obtain them from the unperturbed non-stationary states, which evolve without introducing spurious frequencies [132]. The unperturbed equation for $\tilde{z}(t)$ yields the EOM-UCC eigenvectors and energies, with $\hat{x}(t) = \hat{T}$ and $\partial_t \hat{x} = 0$. The residual operator then becomes $\hat{R}_x(t) = -\hat{H}_T$, where $\hat{H}_T = e^{-\hat{T}} \hat{H}_0 e^{\hat{T}}$. Inserting it into Eq. (20) gives:

$$\langle \left[\hat{\Xi}_{0,\mu} \, , \, \mathrm{i}\partial_t \tilde{z}(t) - [\hat{H}_T, \tilde{z}(t)] \right] \rangle = \langle \left[\hat{\Xi}^{(1)}_{\mu}(t) \, , \, \hat{H}_T \right] \rangle \, , \tag{21}$$

where $\hat{\Xi}_{0,\mu} = \hat{\pi}_T(\hat{\kappa}_\mu)$ is a transformed static basis object. The right-hand side of Eq. (21) is zero, as long as one can express $\hat{\Xi}^{(1)}_{\mu}(t)$ in the basis $\{\hat{\Xi}_{0,\mu}\}$ (which demands algebraic closedness), because ground-state optimization imposes $\langle [\hat{\Xi}_{0,\mu}, \hat{H}_T] \rangle = 0$.

Hence, the unperturbed first-order EOM simplifies to:

$$\langle \left[\hat{\Xi}_{0,\mu} \, , \, \mathrm{i}\partial_t \tilde{z}(t) - [\hat{H}_T, \tilde{z}(t)] \right] \rangle = 0 \, . \tag{22}$$

This equation requires an oscillatory solution. Since the generator $\tilde{z}(t)$ is anti-Hermitian ($\tilde{z}^\dagger(t) = -\tilde{z}(t)$), the fluctuation operator cannot be a single complex exponential; the general solution combines forward ($e^{-\mathrm{i}\Omega_I t}$) and backward ($e^{\mathrm{i}\Omega_I t}$) frequencies. We take the eigen-vectors to be

$$\tilde{X}^I = \sum_\mu X^I_\mu \hat{\Xi}_{0,\mu} \, . \tag{23}$$

The coefficients X^I_μ are complex-valued, so this operator is not anti-Hermitian. Expanding over this basis is convenient as it brings in a metric matrix consistent with the way the solutions to the Dirac-Frenkel problem are treated.

In standard non-Hermitian TD-MRCC, transition elements involve numerical shifts because there are left/right wavefunctions that are different for the same quantum state. The unitary framework can eliminate these. With $\hat{T}$ anti-Hermitian, the Hamiltonian $\hat{H}_T = e^{-\hat{T}} \hat{H}_0 e^{\hat{T}}$ remains Hermitian. Averaging the EOM-UCC relation $[\hat{H}_T, \tilde{X}^I] = \Omega_I \tilde{X}^I$ over the reference gives: $0 = \langle [\hat{H}_T, \tilde{X}^I] \rangle = \Omega_I \langle \tilde{X}^I \rangle$. For regular transitions with $\Omega_I \neq 0$, this gives $\langle \tilde{X}^I \rangle = 0$, which is exact in the closed-algebra cases, and FCI (full configuration interaction) limits. Otherwise $\langle \tilde{X}^I \rangle$ could be small, but nonzero. Although $\langle \hat{\kappa}_\mu \rangle = 0$ by construction of the $\{\hat{\tau}_{\bar{\mu}}\}$ operators, the operators $\hat{\Xi}_{0,\mu} = \hat{\pi}_T(\hat{\kappa}_\mu)$ involve nested commutators with $\hat{T}$, that is, products of these operators whose reference expectations reduce to overlaps. Because the eigenvalue problem and the equations of motion imply only commutators, each $\tilde{X}^I$ is defined up to an additive multiple of the identity. One can fix this freedom, for example, through the convention

$$\tilde{X}^I \leftarrow \tilde{X}^I - \langle \tilde{X}^I \rangle \hat{1} \, , \tag{24}$$

with the adjoint vectors carrying the conjugate constant; both constants drop from every commutator below and are kept implicit hereafter. The constant induced in the generator $\tilde{z}(0)$ (defined below) by this shift is purely imaginary, so anti-Hermiticity is preserved. With this convention, $\langle \tilde{X}^I \rangle = 0$ holds at any truncation order. We invoke this convention below to make statements about $\langle \tilde{z}(0) \rangle$ exact; the calculations reported here do not apply it (Sec. 3.1), but it is important

for supermolecular additivity, as discussed in the supplementary material. In any case, the condition $\langle \tilde{X}^I \rangle = 0$ is stronger than Eq. (24). Now, since the operators $\hat{\Xi}_{0,\mu}$ are anti-Hermitian ($\hat{\Xi}^\dagger_{0,\mu} = -\hat{\Xi}_{0,\mu}$), the adjoint of a given eigenvector is:

$$\tilde{X}^{I\dagger} = \sum_\mu (X^I_\mu)^* \hat{\Xi}^\dagger_{0,\mu} = -\sum_\mu (X^I_\mu)^* \hat{\Xi}_{0,\mu} \ . \tag{25}$$

These relations yield the unperturbed expression:

$$\tilde{z}(t) = \sum_{I>0} \left(c_I e^{-\mathrm{i}\Omega_I t} \tilde{X}^I - c_I^* e^{\mathrm{i}\Omega_I t} \tilde{X}^{I\dagger} \right) \ . \tag{26}$$

The operator $\tilde{z}(t)$ is anti-Hermitian at general truncation orders.

Substituting this expansion into Eq. (22) and grouping the terms with $e^{-\mathrm{i}\Omega_I t}$, we find the EOM-UCC eigenvalue problem:

$$\sum_\nu \langle \left[\hat{\Xi}_{0,\mu} \, , \, \left[\hat{H}_T, \hat{\Xi}_{0,\nu} \right] \right] \rangle X^I_\nu = \Omega_I \sum_\nu \langle \left[\hat{\Xi}_{0,\mu} \, , \, \hat{\Xi}_{0,\nu} \right] \rangle X^I_\nu \ . \tag{27}$$

The terms with $e^{\mathrm{i}\Omega_I t}$ lead to the conjugate problem:

$$-\Omega_I \langle \left[\hat{\Xi}_{0,\mu} \, , \, \tilde{X}^{I\dagger} \right] \rangle = \langle \left[\hat{\Xi}_{0,\mu} \, , \, \left[\hat{H}_T, \tilde{X}^{I\dagger} \right] \right] \rangle \ . \tag{28}$$

The practical matrix eigenvalue problem reads $\mathbf{A}\mathbf{X}^I = \Omega_I \mathbf{S}\mathbf{X}^I$. The Jacobian matrix is $A_{\mu\nu} = \langle [\hat{\Xi}_{0,\mu}, [\hat{H}_T, \hat{\Xi}_{0,\nu}]] \rangle$, and the metric matrix is $S_{\mu\nu} = \langle [\hat{\Xi}_{0,\mu}, \hat{\Xi}_{0,\nu}] \rangle$. Using the Jacobi identity over the commutators gives:

$$A_{\mu\nu} - A_{\nu\mu} = \langle [\hat{\Xi}_{0,\mu}, [\hat{H}_T, \hat{\Xi}_{0,\nu}]] \rangle - \langle [\hat{\Xi}_{0,\nu}, [\hat{H}_T, \hat{\Xi}_{0,\mu}]] \rangle = +\langle [\hat{H}_T, [\hat{\Xi}_{0,\mu}, \hat{\Xi}_{0,\nu}]] \rangle \ . \tag{29}$$

If the commutators close, the right-hand side vanishes, as happens in an FCI-style calculation or under $\mathfrak{su}(M)$ adaptation; otherwise one symmetrizes the Jacobian by hand, $\mathbf{A} \leftarrow (1/2)(\mathbf{A} + \mathbf{A}^\dagger)$.

With either route, the Jacobian is symmetric ($A_{\mu\nu} = A_{\nu\mu}$), and the metric matrix anti-symmetric ($S_{\mu\nu} = -S_{\nu\mu}$). The projection can then be carried out with the adjoint vector $\tilde{X}^{I\dagger}$, so no separate left-hand operators are needed. Evaluated at $t = 0$, the unperturbed solution gives the initial condition for $\tilde{z}$:

$$\tilde{z}(0) = \sum_{I>0} \left(c_I \tilde{X}^I - c_I^* \tilde{X}^{I\dagger} \right) \ . \tag{30}$$

The coefficients $\{c_I\}$ are the linear (complex) amplitudes of the initial state.

2.5 Propagation of Linear Superpositions

Let us consider $\hat{U}_{\mathrm{QM}}(t)$ as the conventional full quantum mechanical evolution operator, $\hat{U}_{\mathrm{QM}}(t) = \mathcal{T} \exp(-\mathrm{i} \int_0^t \hat{H}(s) \mathrm{d}s)$. Its action is reproduced by a CC propagator, denoted $\hat{U}_y(t)$, which unlike the full QM operator depends on the initial state. The generator of the previous subsection acts like a rotation of the reference. Consider a general coherent initial state, expressed in terms of a (complex) ground-state amplitude c_0 and a static, anti-Hermitian operator $\tilde{z}(0)$ acting upon the correlated UCC ground state. The resulting propagated state is written as:

$$\begin{aligned} |\Psi(t)\rangle &= \hat{U}_{\mathrm{QM}}(t) e^{\hat{T}} [c_0 + \tilde{z}(0)] |0\rangle \ , \\ &= \hat{U}_y(t) [c_0 + \tilde{z}(0)] |0\rangle \ , \end{aligned} \tag{31}$$

$\tilde{z}(0)$ describes the excited-state superposition component of the overall initial state; $c_0 = 0$ is a valid value. Because $\hat{U}_y(t)$ describes the time dependence, observables follow from the Heisenberg-like operator $\tilde{B}_y(t) = \hat{U}_y^\dagger(t)\hat{B}\hat{U}_y(t)$, giving:

$$\langle\hat{B}\rangle(t) = \frac{\langle[c_0^* - \tilde{z}(0)]\tilde{B}_y(t)[c_0 + \tilde{z}(0)]\rangle}{|c_0|^2 + \langle -\tilde{z}^2(0)\rangle} \ . \tag{32}$$

The minus sign is only a reflection of Hermiticity, but norms are strictly positive. The denominator is the squared norm $\langle\bar{\Psi}(0)|\bar{\Psi}(0)\rangle$ ($|\bar{\Psi}(0)\rangle = [c_0 + \tilde{z}(0)]|0\rangle$), where the cross terms $c_0^*\langle\tilde{z}(0)\rangle - c_0\langle\tilde{z}(0)\rangle$ vanish identically. $\tilde{z}(0)$ is a sum of nonzero-frequency EOM-UCC vectors $\tilde{X}^I$ and their adjoints, and the reference-component convention of Eq. (24) enforces $\langle\tilde{X}^I\rangle = 0$, hence $\langle\tilde{z}(0)\rangle = 0$ (Sec. 2.4). Because $\tilde{z}(0)$ is static, these observables should not diverge, which can be seen if the above is rewritten as

$$\begin{aligned}\langle\hat{B}\rangle(t) = \langle\tilde{B}_y(t)\rangle + \frac{1}{|c_0|^2 + \langle -\tilde{z}^2(0)\rangle}\Big(&c_0^*\langle\tilde{B}_y(t)\tilde{z}(0)\rangle - c_0\langle\tilde{z}(0)\tilde{B}_y(t)\rangle \\ &+ \frac{1}{2}\langle[[\tilde{B}_y(t), \tilde{z}(0)], \tilde{z}(0)]\rangle - \frac{1}{2}\langle\{\tilde{B}_y(t), \tilde{z}^2(0)\}\rangle_{\mathrm{C}}\Big) \ .\end{aligned} \tag{33}$$

Only benign commutators and their "anti" forms appear. The normalization factor is formally present because we normalize with respect to the metric matrix of the EOM-UCC problem.

The propagator is given by a time-dependent, anti-Hermitian cluster operator $\hat{y}(t)$, with $\hat{U}_y(t) = \exp[\hat{y}(t)]$, $\hat{y}(t=0) = \hat{T}$, and no parameter g employed in this case. Applying the Dirac-Frenkel action principle to this superposition reference yields the working equation (it reduces to Eq. (11) when $\tilde{z}(0) = 0$):

$$\langle\bar{\Psi}(0)|\left[\hat{\Xi}_{y,\mu}(t)\,,\,\hat{R}_y(t)\right]|\bar{\Psi}(0)\rangle = 0 \ . \tag{34}$$

The transformed basis element reads $\hat{\Xi}_{y,\mu}(t) = \hat{\pi}_{y(t)}(\hat{\kappa}_\mu)$, and the residual is $\hat{R}_y(t) = \mathrm{i}\hat{\pi}_y(\partial_t\hat{y}(t)) - \hat{H}_y(t)$, with $\hat{H}_y(t) = e^{-\hat{y}(t)}\hat{H}(t)e^{\hat{y}(t)}$.

Finally, let us assume that $\hat{H}(-t) = \hat{H}(t)$. The generator is anti-Hermitian at all times,

$$\hat{y}^\dagger(t) = -\hat{y}(t) \ , \tag{35}$$

so $\hat{U}_y(t) = e^{\hat{y}(t)}$ is unitary. In Eq. (34), the sign flips of i and of ∂_{-t} cancel in $\mathrm{i}\hat{\pi}_y(\partial_t\hat{y})$, so complex conjugation combined with $t \to -t$ leads to a solution generated by the conjugated reference,

$$\left[\hat{y}_{\bar{\Psi}}(t)\right]^* = \hat{y}_{\bar{\Psi}^*}(-t) \ , \tag{36}$$

with the subindex indicating conjugation of the starting reference state. The initial condition is the same because $\hat{T}^* = \hat{T}$. For a real observable $\hat{B}$, the numerator of Eq. (32) is real by Eq. (35) and is carried to the conjugated reference by Eq. (36), while the denominator is a norm, so

$$\langle\hat{B}\rangle_{\bar{\Psi}}(-t) = \langle\hat{B}\rangle_{\bar{\Psi}^*}(t) \ . \tag{37}$$

As long as the references are related by a global phase, $|\bar{\Psi}^*(0)\rangle \propto |\bar{\Psi}(0)\rangle$, the two sides relate to each other and Eqs. (36) and (37) reduce to $\hat{y}(-t) = \hat{y}^*(t)$ and $\langle\hat{B}\rangle(-t) = \langle\hat{B}\rangle(t)$.

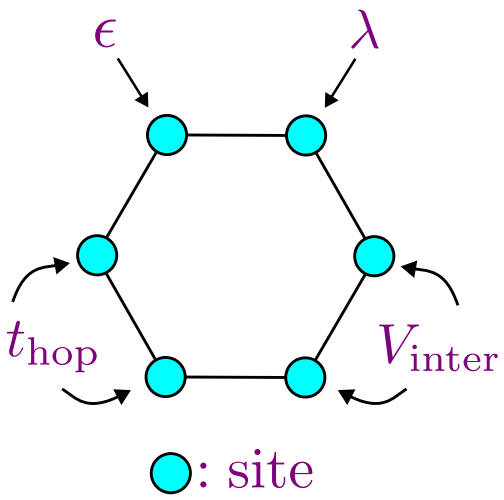

Figure 1. Sketch of the model, a six-site ring ($L = 6$) with inter-site coupling (V_{inter}), on-site energy (ϵ), on-site linear source field strength (λ), and inter-site hopping (t_{hop}). Each site carries a hard-core boson and is therefore in a "0" or "1" state, mimicking a neutral-atom cluster.

3 Numerical Simulation Details

3.1 Bose-Hubbard Model and Interaction Picture Solution

To implement the equations of motion computationally, we consider a finite-dimensional matrix representation [130, 133], and define a 1D hard-core bosonic model, depicted in Fig. 1. The time-dependent Hamiltonian reads:

$$\hat{H}(t) = \hat{H}_0 - f(t)\hat{\mu} \ , \tag{38}$$

where $\hat{H}_0$ spans L interacting sites arranged on a ring:

$$\hat{H}_0 = \epsilon \sum_{j=1}^{L} \hat{n}_j + V_{\mathrm{inter}} \sum_{j=1}^{L} \hat{n}_j \hat{n}_{j+1} + t_{\mathrm{hop}} \sum_{j=1}^{L} \left(\hat{b}_j^\dagger \hat{b}_{j+1} + \hat{b}_{j+1}^\dagger \hat{b}_j \right) + \lambda \sum_{j=1}^{L} \left(\hat{b}_j^\dagger + \hat{b}_j \right) \ . \tag{39}$$

The operators $\hat{b}_j^\dagger$ and $\hat{b}_j$ are the creation and annihilation operators at site j, and $\hat{n}_j = \hat{b}_j^\dagger \hat{b}_j$ (the boson number operator); each site can hold at most one boson. These operators follow $(\hat{b}_j)^2 = (\hat{b}_j^\dagger)^2 = 0$, $[\hat{b}_i, \hat{b}_j^\dagger] = \delta_{ij}(1 - 2\hat{n}_j)$, and $[\hat{b}_i, \hat{b}_j] = [\hat{b}_i^\dagger, \hat{b}_j^\dagger] = 0$ for all i, j. This numerical application thus exercises non-commutativity between $\hat{\tau}_{\bar{\mu}}^\dagger$ and $\hat{\tau}_{\bar{\nu}}$ (implying non-commutativity among $\hat{\kappa}_\mu$ objects or $\hat{\Xi}_{0,\mu}$ objects), but not between pairs like $(\hat{\tau}_{\bar{\mu}},\ \hat{\tau}_{\bar{\nu}})$ or $(\hat{\tau}_{\bar{\mu}}^\dagger,\ \hat{\tau}_{\bar{\nu}}^\dagger)$, $\bar{\mu} \neq \bar{\nu}$. These properties prevent natural truncation of the BCH series.

The on-site energy is ϵ, t_{hop} is the hopping parameter, V_{inter} the nearest-neighbor repulsion term, and λ is an on-site source field strength. Periodic boundary conditions are imposed as $\hat{b}_{L+1} \equiv \hat{b}_1$, so that the interaction and hopping terms close the chain into a ring. The term involving λ breaks boson-number conservation (or excitation conservation). The constant shift of the EOM vectors, Eq. (24), serves a theoretical purpose, but it is not required for the calculations below. This point is further discussed below and in the supplementary material. There we also show details about the reference construction, which is constructed by including the no-boson state and all the single-boson configurations. The reference state $|0\rangle$ is built by diagonalizing the static Hamiltonian $\hat{H}_0$ over those configurations and selecting $|0\rangle$ as the lowest-energy state.

It is convenient to switch to the interaction picture. To this end we write $|\Psi(t)\rangle = e^{-\mathrm{i}\hat{H}_0 t}\hat{U}_{\mathrm{I}}(t)[c_0 + \tilde{z}(0)]|0\rangle$, and define $\hat{V}_{\mathrm{I}}(t) = e^{\mathrm{i}\hat{H}_0 t}\hat{V}(t)e^{-\mathrm{i}\hat{H}_0 t}$, where

$\hat{V}(t) = -f(t)\hat{\mu}$. The UCC operator reads $\hat{U}_{\rm I}(t) = \exp[\hat{y}_{\rm i}(t)]$, with $\hat{y}_{\rm i}(t=0) = \hat{T}$. The new "$\Xi$" term is $\hat{\Xi}_{{\rm I},\mu}(t) = \hat{\pi}_{y_{\rm i}}(\hat{\kappa}_\mu)$. Based on these definitions, and the expansion $\hat{y}_{\rm i}(t) = \sum_\mu y_{{\rm i},\mu}(t)\hat{\kappa}_\mu$, the numerical equation to solve takes the form:

$$\sum_\nu {\rm Im}[S'_{\mu\nu}(t)]\dot{y}_{{\rm i},\nu} = -{\rm Re}[h_{{\rm eff},\mu}(t)] \ , \tag{40}$$

where $S'_{\mu\nu} = \langle\bar{\Psi}(0)|\hat{\Xi}_{{\rm I},\mu}(t)\hat{\Xi}_{{\rm I},\nu}(t)|\bar{\Psi}(0)\rangle$, and $h_{{\rm eff},\mu}(t) = \langle\bar{\Psi}(0)|\hat{\Xi}_{{\rm I},\mu}(t)e^{-\hat{y}_{\rm i}(t)}\hat{V}_{\rm I}(t)e^{\hat{y}_{\rm i}(t)}|\bar{\Psi}(0)\rangle$. Observables are evaluated using Eq. (32) after setting $\hat{U}_y(t) = e^{-{\rm i}\hat{H}_0 t}e^{\hat{y}_{\rm i}(t)}$. Our formulation is based on Heisenberg-type matrix mechanics, with all operators represented in the $\{|\bar{\mu}\rangle\}$ basis. The exponential maps and $\hat{\pi}$ superoperators are evaluated using the spectral theorem and its functional calculus. These avoid truncation errors, and are efficient for the system treated here.

We apply a Gaussian pulse to study the time-evolution of the system. For $t \geq 0$, the time-dependent field is:

$$f(t)\hat{\mu} = f_0 \exp\left(-\frac{(t-t_0)^2}{2\sigma^2}\right)\mu_0 \sum_{j=1}^{L}\left(\hat{b}_j^\dagger + \hat{b}_j\right) \ . \tag{41}$$

For a numerical simulation over a ring of $L = 6$ sites, we use the following parameters: $\epsilon = 1.0$ eV, $V_{\rm inter} = 0.500$ eV, $t_{\rm hop} = 0.050$ eV, $\lambda = 0.200$ eV (equivalently 0.03675, 0.01838, 0.001838, and 0.00735 a.u.), $\mu_0 = 0.25$ a.u., $f_0 = 0.25$ a.u., $\sigma = 50$ a.u., and $t_0 = 150$ a.u. The simulation covers the time interval $t \in [0, 500]$ a.u.

3.2 Piecewise Propagation

Under strong driving, continuous propagation of the cluster operator $\hat{y}_{\rm i}(t)$ can drive the amplitudes to large values. In a truncated UCC space, heavily displaced generators amplify the out-of-subspace truncation errors inherent to the BCH expansion. To keep the interaction-picture amplitudes bounded, and prevent "degradation" of the metric as well, we introduce a piecewise restart protocol that re-centers the reference frame. Consider the interaction-picture state vector at an absolute propagation time t, Eq. (31). When the integration reaches a boundary time τ, the state is evaluated as $|\Psi(\tau)\rangle = e^{-{\rm i}\hat{H}_0\tau}\hat{U}_{y_{\rm i}}(\tau)|\bar{\Psi}(0)\rangle$. At this point, the history of the wave packet is absorbed into an updated reference state, $|\bar{\Psi}(0)\rangle \leftarrow e^{-{\rm i}\hat{H}_0\tau}\hat{U}_{y_{\rm i}}(\tau)|\bar{\Psi}(0)\rangle$. The time-independent reference Hamiltonian is then shifted to include the external potential at $t = \tau$, $\hat{H}_0 \leftarrow \hat{H}_0 + \hat{V}(\tau)$. To strictly preserve the total physical Hamiltonian, $\hat{H}(t) = \hat{H}_0^{(\rm new)} + \hat{V}^{(\rm new)}(t)$, the time-dependent interaction potential for the subsequent interval must be redefined as the residual fluctuation: $\hat{V}(t) \leftarrow \hat{V}(t) - \hat{V}(\tau)$, so that the effective perturbation starts from zero in the new epoch ($\hat{V}(\tau) = 0$).

The local time coordinate is reset by $t \leftarrow t - \tau$. Because the new reference $|\bar{\Psi}(0)\rangle$ is the physical state at the boundary, the dynamic cluster operator for the new interval must be the identity, $\hat{y}_{\rm i}(0^+) = 0$. For propagation in the new time slot, the state is evaluated using the new relative time t as $|\Psi(t)\rangle = e^{-{\rm i}\hat{H}_0 t}\hat{U}_{y_{\rm i}}(t)|\bar{\Psi}(0)\rangle$, where $\hat{H}_0$, $\hat{V}(t)$, and $|\bar{\Psi}(0)\rangle$ carry their newly updated values. In an untruncated space or closed algebraic system, the BCH expansion is closed, while the piecewise evaluation matches the continuous single-exponential ansatz. Otherwise, the consecutive piecewise layers generate higher-order, out-of-basis terms through the nested commutators of the BCH series.

4 Results and Discussion

4.1 Numerical

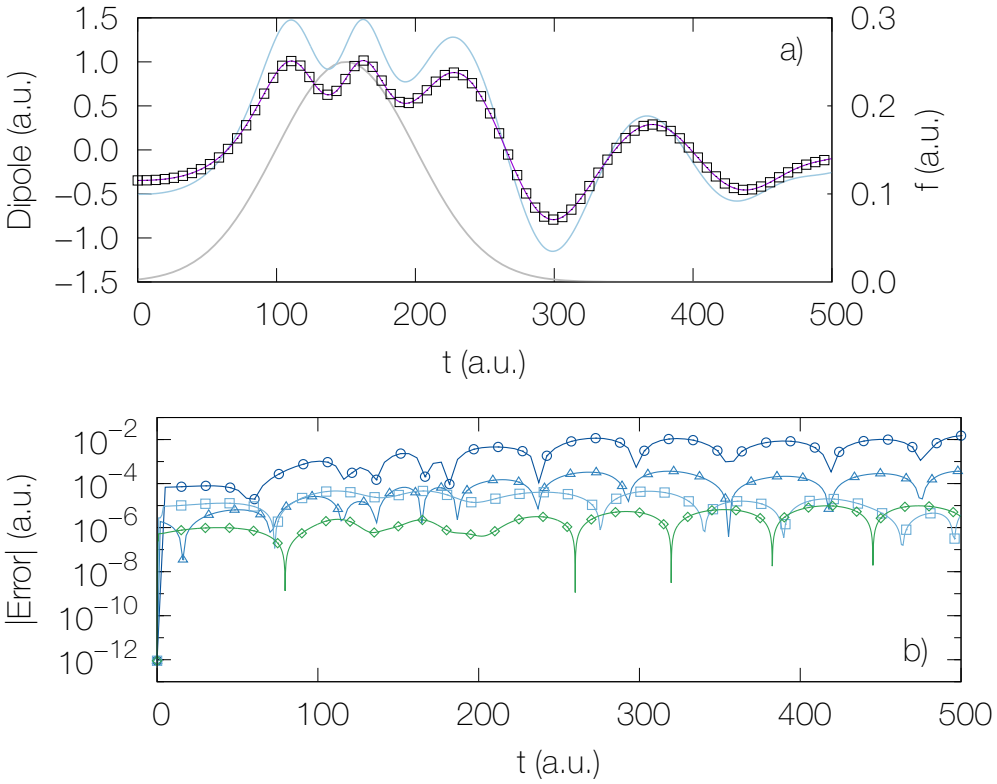

Figure 2. a) Time-dependent dipole of the LC-initiated state (dark violet line, TDUCC; black open squares, FCI), together with the ground-state-initiated dipole μ_{00} (light blue) and, on the right-hand axis, the Gaussian driving field $f(t)$ (grey). b) Absolute deviation $|\mu^{\mathrm{UCC}}(t) - \mu^{\mathrm{FCI}}(t)|$ of the LC-initiated dipole, on a logarithmic scale, for four step counts over the same window $t \in [0, 500]$ a.u.: $N_t = 100$ (dark blue, open circles), 250 (medium blue, open triangles), 500 (light blue, open squares) and 5000 (green, open diamonds).

We test the TD-UCC approach on the hard-core boson model of Sec. 3.1. For the driven dipole, the state populations, a dipole-dipole correlation function, and the reference-excited coherence, the deviation from the exact propagation for fine time-step simulations stays at or below 10^{-5}, against signals of order 10^{-1}. The two-time correlation function is a quantity examined here for which the theory is not exact; we treat it separately below. The following discussion focuses on expectation values (static matrix elements such as $\langle\Psi_I|\hat{B}|\Psi_J\rangle$ can be deduced from Eq. (33), as discussed in the supplementary material).

Figure 2 shows the dipole under the external driving field. Panel (a) gives the non-linear dipole dynamics obtained by propagating a linear combination (LC) superposition state, with $c_0 = 1/\sqrt{17}$ and $\tilde{z}(0) = c_1(\tilde{X}^1 - \tilde{X}^{1\dagger})$, $c_1 = 4/\sqrt{17}$; the ground-state-initiated dipole (from $e^{\hat{T}}|0\rangle$) is shown as a reference curve and the Gaussian driving field $f(t)$ appears on the right-hand axis. The initial superposition produces a non-stationary response of amplitude 0.35 a.u., which the unitary coupled-cluster framework reproduces in comparison to the FCI propagation. Figure 2(b) gives the absolute deviation between the UCC and FCI dipoles for the LC-initiated state at four step counts over the same 500 a.u. window.

We observe behavior common to RK4 integrators, with an exception. Going from $N_t = 100$ to 250 steps divides the peak error by 41, close to the 39 expected from $(2.5)^4$, lowering from 1.5×10^{-2} to 3.6×10^{-4} a.u. Beyond $N_t \approx 10^3$ the scaling

stops. The time-averaged error settles around the order of 10^{-6} a.u., where a fivefold refinement for $N_t = 5000$ makes the peak error improve by less than a factor of 1.5. The error is not uniform within a single propagation; it collapses at the nodes of the response, down to 1×10^{-9} a.u. against a peak of 1×10^{-5} a.u. The instantaneous error value spans more than four orders of magnitude. Such behavior is familiar in TD unitary theories. During the RK4 propagation the rates $\dot{y}_{\mathrm{i},\mu}$ follow from the real linear system $\sum_\nu \mathrm{Im}[S'_{\mu\nu}(t)]\, \dot{y}_{\mathrm{i},\nu} = -\mathrm{Re}[h_{\mathrm{eff},\mu}(t)]$. Depending on the driven state and the active basis, the coefficient matrix $\mathrm{Im}[S(t)]$ can be subject to ill conditioning. Increasing the number of steps is not sufficient to reduce further the error. After the propagation starts the metric matrix can introduce numerical noise. In this case, we use complete orthogonal decomposition for the solution of the linear problem. With solver pivot tolerance of 10^{-8} the RK4 accuracy does not improve much beyond 500 timesteps, whereas with 10^{-9} we see a more systematic error reduction. However, further reducing the COD threshold does not improve the error and can revert the trend, evidencing the expected issue with the metric matrix. These results suggest that such matrix needs to be well characterized for robust propagations based on it. There are potentially multiple pathways to improve stability, such as rotation of the reference (but these are unexplored in this work).

Regarding Fig. 2(a), the ground-state-initiated and LC-initiated dipoles follow similar oscillation profiles, despite the very different initial states. The reason is connected to the couplings and translational symmetry. The dipole $\hat{\mu} = \mu_0 \sum_{j=1}^{L} (\hat{b}_j^\dagger + \hat{b}_j)$ is a spatially uniform, single collective coordinate, and the driving field couples to it alone, which is related to the generalized Kohn theorem. The ground state and the LC superposition differ only in the internal interactions (due to V_{inter}), which $\hat{\mu}$ does not capture, so the two dipole signals reduce to a similar collective response, separated by an approximate amplitude prefactor.

Figure 3 shows the time evolution of the state coherence $c_0(t)c_1^*(t)$. Over the considered time window the coherence departs from the exact result by at most 4.4×10^{-5} against an amplitude of 0.24, and the excited- and ground-state populations by at most 2×10^{-5}. Coherences require more work to track in non-Hermitian methods, where imbalances between the left and right states introduce the mentioned asymmetrical residues. Here the bra and ket come from the same norm-preserving unitary map, and the deviation in the bottom panel oscillates about a slowly rising envelope. The coherence error repeats the pattern of the dipole with a shallower initial slope. The peak deviation falls from 8×10^{-3} at $N_t = 100$ to 7×10^{-4} at $N_t = 250$, then to 2×10^{-4} at $N_t = 500$ and 4×10^{-5} at $N_t = 1000$, close to second-order scaling, and finally stalls at 4×10^{-5} when the grid is refined to $N_t = 5000$.

The time evolution of the correlation function, defined as $C_{\mathrm{dd}}(t) = \langle \bar{\Psi}(0)|\hat{\mu}(t)\hat{\mu}(0)|\bar{\Psi}(0)\rangle$ (where $\hat{\mu}(t) = \hat{U}_{\mathrm{QM}}^\dagger(t)\hat{\mu}\hat{U}_{\mathrm{QM}}(t)$), is presented in Fig. 4. Two propagated states determine this quantity: i) the left (bra) factor is the ordinary state evolved in this work, while ii) the right (ket) factor is initialized by the dipole acting on the correlated state, $\hat{\mu}\, e^{\hat{T}}|\bar{\Psi}(0)\rangle$, or $\bar{\mu}|\bar{\Psi}(0)\rangle = e^{-\hat{T}}\hat{\mu}\, e^{\hat{T}}|\bar{\Psi}(0)\rangle$ as used here, and then evolved forward. The present formalism is not exact for this quantity; we include the figure to show that limitation. The interaction-picture generator $\hat{y}_{\mathrm{i}}(t)$ is built to propagate the physical superposition state $[c_0 + \tilde{z}(0)]|0\rangle$, which the "dipole-kicked" ket $\hat{\mu}\, e^{\hat{T}}|\bar{\Psi}(0)\rangle$ is not. We note that the deviation stops responding to the time step. Refining the grid from $N_t = 250$ to $N_t = 5000$ moves the peak deviation from 1.2×10^{-2} to 1.4×10^{-2} a.u.

Figure 5 tracks the cluster generator norms and tests the piecewise propagation

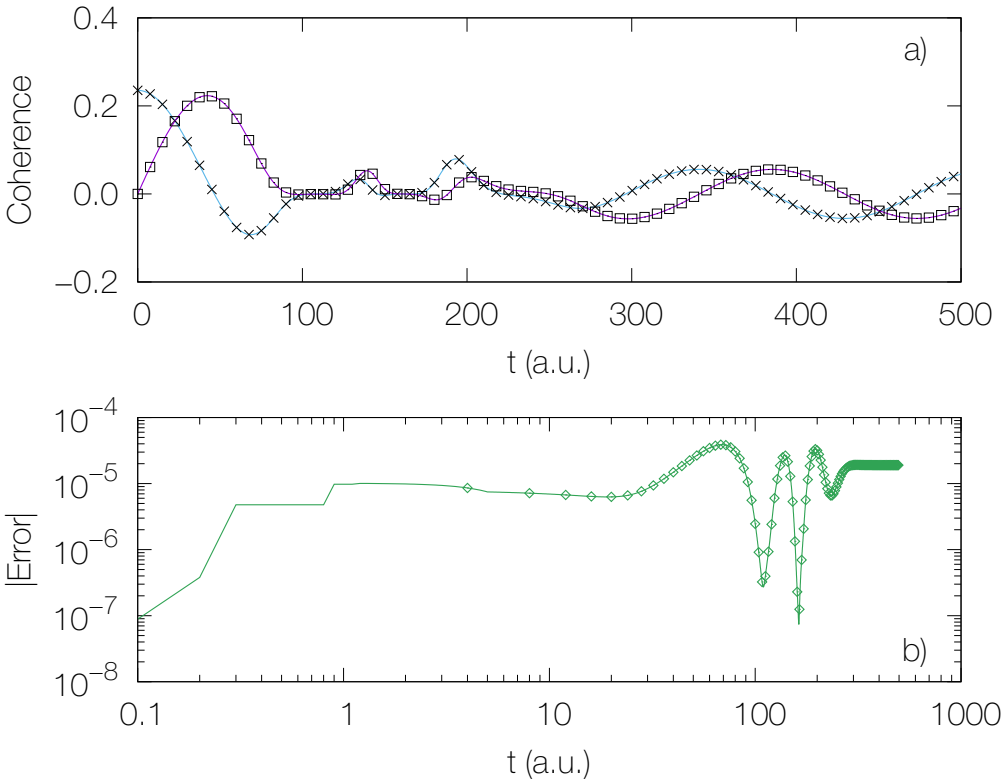

Figure 3. a) Time evolution of the coherence $c_0(t)c_1^*(t)$ between the reference and the lowest excited state: real part (sky blue line, TDUCC; black crosses, FCI) and imaginary part (dark violet line, TDUCC; black open squares, FCI). b) Absolute deviation of the coherence from the exact reference, on logarithmic axes, for the finest grid ($N_t = 5000$ steps over $t \in [0, 500]$ a.u.).

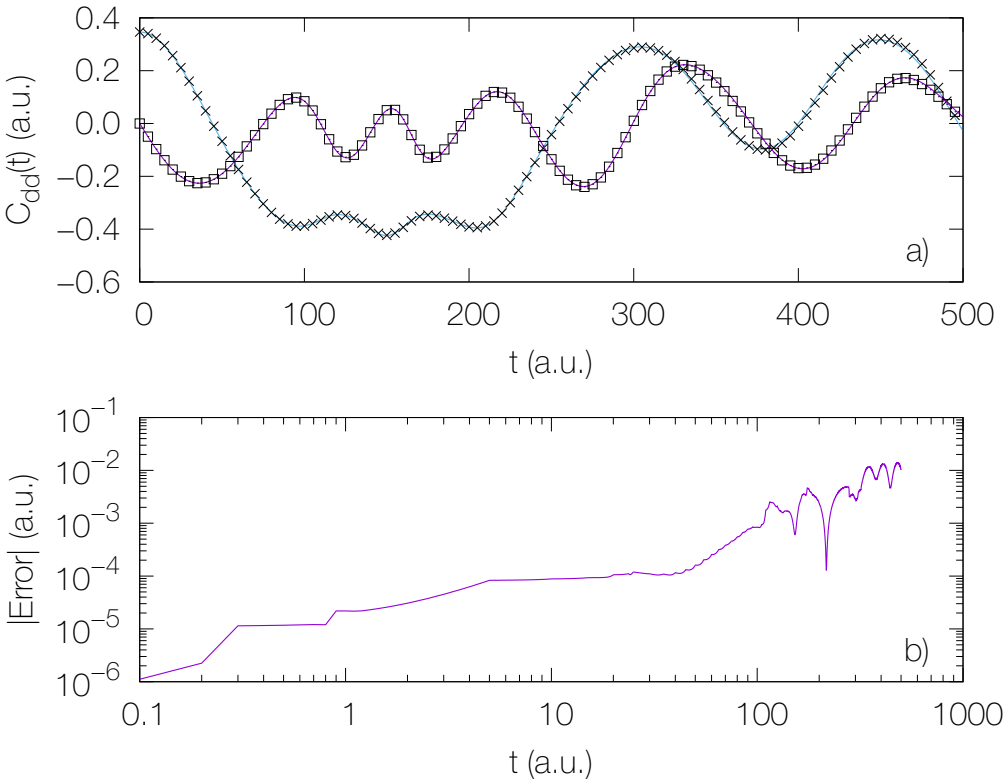

Figure 4. a) Time evolution of the dipole correlation function $C_{\mathrm{dd}}(t) = \langle\bar{\Psi}(0)|\hat{\mu}(t)\hat{\mu}(0)|\bar{\Psi}(0)\rangle$; real part (sky blue line, TDUCC; black crosses, FCI) and imaginary part (dark violet line, TDUCC; black open squares, FCI). b) Absolute deviation $|C_{\mathrm{dd}}^{\mathrm{UCC}}(t) - C_{\mathrm{dd}}^{\mathrm{FCI}}(t)|$ from the exact reference, on logarithmic axes, for the finest grid ($N_t = 5000$ steps over $t \in [0, 500]$ a.u.).

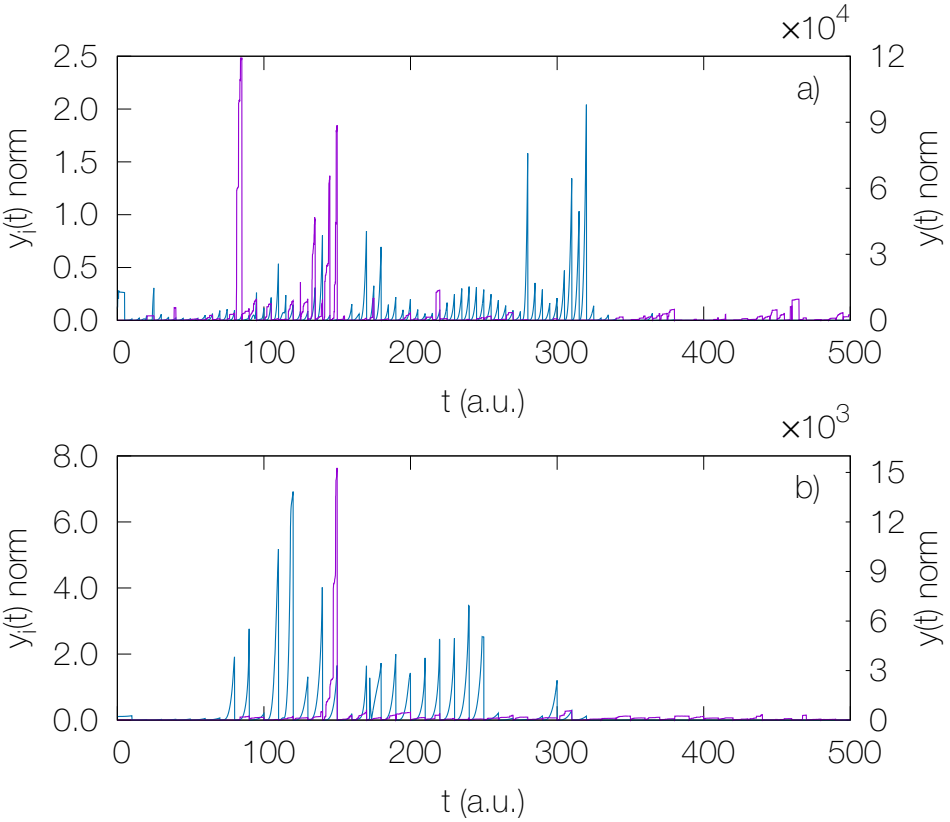

Figure 5. Time-dependent cluster generator norms under the piecewise restart protocol of Sec. 3.2, for $N_t = 5000$ steps over $t \in [0, 500]$ a.u. Left-hand axis: the interaction-picture generator norm $\|\hat{y}_i(t)\|$ (blue), reset to zero at every restart and therefore tracing a sawtooth; right-hand axis: $\|\hat{y}(t)\|$ (dark violet), rescaled by the common factor annotated at the top right of each panel. a) 100 restart epochs, where $\|\hat{y}_i\|$ stays below 2.1; b) 50 epochs, where it reaches 6.9.

protocol of Sec. 3.2. As the external field drives the system away from its original state, the continuous cluster amplitudes grow. Over this window $\|\hat{y}(t)\|$ reaches 1.2×10^5. Each restart absorbs the accumulated amplitudes into an updated reference state and resets the generator to zero, so the interaction-picture norm $\|\hat{y}_\mathrm{i}(t)\|$ traces the sawtooth seen in both panels. With 100 time-intervals the norm never exceeds 2.1; with 50 intervals it reaches 6.9. Doubling the interval between restarts costs a factor of three in the quantity the procedure controls. A small generator keeps the BCH expansion in the regime where the truncated algebra could be a good approximation, which limits metric degradation and keeps long propagations stable under strong driving. These results suggest that the solution to the TD-UCC derived here should be adaptive. In other simulations with lower external couplings, we noted that even one single interval for the whole propagation is sufficient, reinforcing the idea that adaptation is required based on the operator norms. An improved adaptive method does not necessarily mean that one has to work in the interaction picture; in preliminary tests we also find cases where $\hat{y}(t)$ is numerically bounded in an appropriate manner, whereas $\hat{y}_\mathrm{i}(t)$ is not (these will be investigated in the future).

For the numerical cases above we find that $\|\tilde{X}^{I\dagger}|0\rangle\|/\|\tilde{X}^I|0\rangle\| \approx 10^{-14}$: the annihilating condition holds to machine precision. The term $\tilde{z}(0)|0\rangle$ reduces to its forward component $\sum_I c_I \tilde{X}^I|0\rangle$. This is a property of the model considered here due to the condition $\hat{b}^\dagger|1\rangle = 0$, and the type of excitation operator used here, which is basically the boson creation operator that the Hamiltonian relies heavily on (in realistic cases the Hamiltonian is more complex). The anti-Hermitian generator, however, still plays a dominant role in the dynamics since its stationary condition and EOM-UCC equations lead to the construction of the initial state. To obtain explicit contributions from $\tilde{X}^{I\dagger}|0\rangle$, we detune the ground-state cluster operator as $\hat{T}' = \lambda_\mathrm{d}\hat{T}$, where $\hat{T}$ is the correctly converged cluster operator used before. The EOM-UCC problem is then solved using the $\hat{T}'$-transformed static Hamiltonian, and the TD simulation is run with the resulting eigen-vectors/eigen-energies. For $\lambda_\mathrm{d} = 0.75$ we observe (Fig. 6) dipole errors on the order of 10^{-3}, which are then raised to around 10^{-2} at envelope level for $\lambda_\mathrm{d} = 0.5$. This error sustains itself for $\lambda_\mathrm{d} = 0$. These show that the construction of the initial state through the generator $\tilde{z}(0)$ is a viable pathway to approximate observables. The norms $\|\tilde{X}^{I\dagger}|0\rangle\|/\|\tilde{X}^I|0\rangle\|$ here are 8×10^{-3}, 2×10^{-2}, and 3×10^{-2} for $\lambda_\mathrm{d} = 0.75$, $\lambda_\mathrm{d} = 0.5$, and $\lambda_\mathrm{d} = 0$, respectively. In addition, we remark that the object $\tilde{z}(0)$ exists as an anti-Hermitian operator and dynamics originator regardless of detuning; this is due to its definition involving $\tilde{X}^{I\dagger}$ as a general operator.

4.2 Theoretical

In general, the conjugate vector $\tilde{X}^{I\dagger}$ enters the superposition generator as a consequence of the anti-Hermitian restriction. Each $\hat{\kappa}_\mu$ combines an excitation $\hat{\tau}_{\bar{\mu}}$ with its de-excitation $\hat{\tau}^\dagger_{\bar{\mu}}$. Every forward vector carries its adjoint, and through the nested commutators with $\hat{T}$ this adjoint does not annihilate the reference. Because the $\hat{\Xi}_{0,\mu}$ are anti-Hermitian as well, $\tilde{X}^{I\dagger}$ lies in the same excitation space as $\tilde{X}^I$. This pairing recalls the X/Y amplitudes of RPA and TDHF, where de-excitations couple to correlations already present in the ground state. The resemblance is also noted with the eigenvalue problem $\mathbf{A}\mathbf{X}^I = \Omega_I \mathbf{S}\mathbf{X}^I$. The symmetric Jacobian together with the antisymmetric metric $\langle[\hat{\Xi}_{0,\mu}, \hat{\Xi}_{0,\nu}]\rangle$ yields a symplectic spectrum in $\pm\Omega_I$ pairs, with $\tilde{X}^I$ and $\tilde{X}^{I\dagger}$ acting as the forward/backward partners collected into the static

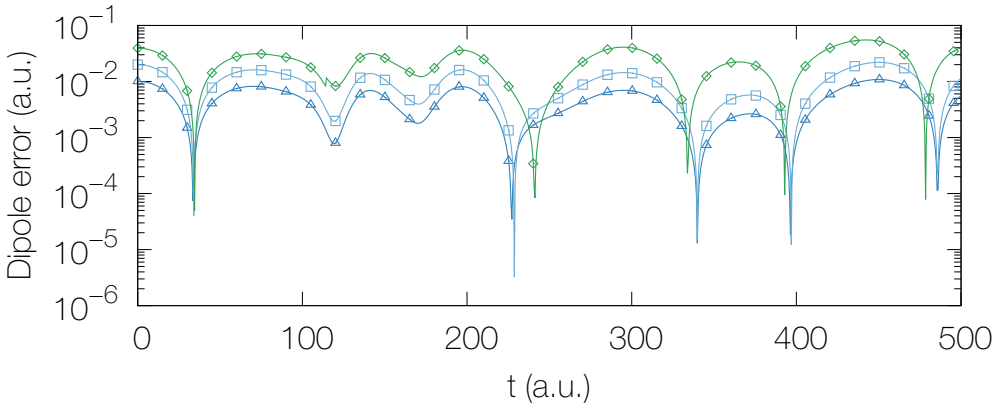

Figure 6. TD dipole error, $|\mu^{\mathrm{UCC}}(t) - \mu^{\mathrm{FCI}}(t)|$, of the LC-initiated dipole, on a logarithmic scale, for the detuned EOM-UCC problem, based on $\hat{T}'$ (this cluster operator is used for the rest of the simulation after solving for the eigenvalues). Time window $t \in [0, 500]$ a.u., 1000 time-steps. Results for $\lambda_{\mathrm{d}} = 0.75$ (medium blue, open triangles), $\lambda_{\mathrm{d}} = 0.5$ (light blue, open squares) and $\lambda_{\mathrm{d}} = 0$ (green, open diamonds).

operator $\tilde{z}(0) = \sum_{I>0}(c_I \tilde{X}^I - c_I^* \tilde{X}^{I\dagger})$. The algebraic form of Eq. (27) is known: it shows a double commutator against an antisymmetric metric, which after the symmetrization noted above is the equation-of-motion method of Rowe [134] with $\hat{H} \to \hat{H}_T$. The eigenvalue problem here, however, arises as the unperturbed limit of the variational equation (20), forming the basis onto which to project, $\hat{\Xi}_{0,\mu} = \hat{\pi}_T(\hat{\kappa}_\mu)$.

For dynamics the above does not hold. The propagator $\hat{U}_y(t)$ is applied to the frozen reference, as opposed to a linear superposition of $e^{\mp \mathrm{i}\Omega_I t}$ terms, so no explicit $e^{+\mathrm{i}\Omega_I t}\tilde{X}^{I\dagger}|0\rangle$ term is propagated. The eigenrelation $[\hat{H}_T, \tilde{X}^I] = \Omega_I \tilde{X}^I$, the operator form of Eq. (27), is applied to the correlated reference and is exact only in the closed-algebra cases or FCI limits, whereas RPA usually restricts its eigenvalue problem to single excitations based on an uncorrelated stationary state. The metric $S'_{\mu\nu}(t) = \langle \bar{\Psi}(0)|\hat{\Xi}_{\mathrm{I},\mu}(t)\hat{\Xi}_{\mathrm{I},\nu}(t)|\bar{\Psi}(0)\rangle$ also follows the propagated basis in time, while the RPA metric is computed once over the frozen reference and stays fixed. We keep the non-annihilating adjoint, since it arises from the anti-Hermitian construction itself, and can be used to investigate linkedness and algebra closedness. If the closure involves the Hamiltonian itself, it can be quite beneficial for size-extensivity, even from the configuration interaction perspective.

Because $\tilde{X}^{I\dagger}|0\rangle \neq 0$ in general for truncated/approximated cases, the "vacuum variance" $\langle -\tilde{z}^2(0)\rangle$ is a required term. A direct expansion of Eq. (32) involves the product $\langle \tilde{z}^2(0)\rangle\langle \tilde{B}_y(t)\rangle$, which can be cancelled out. Given the property $\tilde{z}^\dagger = -\tilde{z}$, the quadratic contribution is $\tilde{z}(0)\tilde{B}_y(t)\tilde{z}(0)$, the same operator on both sides, and it splits into a double commutator and an anticommutator; the form $\tilde{z}^\dagger \tilde{B}_y \tilde{z}$ would not. The commutator $\langle[[\tilde{B}_y(t), \tilde{z}(0)], \tilde{z}(0)]\rangle$ is connected. In the anticommutator, the fully disconnected part cancels against the normalization denominator $|c_0|^2 + \langle -\tilde{z}^2(0)\rangle$, and any term containing an isolated $\tilde{z}(0)$ factor vanishes because of the requirement $\langle \tilde{z}(0)\rangle = 0$. The surviving contributions are therefore connected, $\langle\{\tilde{B}_y(t), \tilde{z}^2(0)\}\rangle_{\mathrm{C}}$. Over the reference $e^{\hat{T}}|0\rangle$ they reduce, through generalized Wick contraction [135, 136], to cumulants of the reference density matrices, so Eq. (33) is linked in the many-body sense, where closed "vacuum" factors drop out and open disconnected cumulants are kept. The cumulants are well-behaved as long as they feature the correct locality.

Truncating the excitation manifold has consequences of algebraic and numerical character. A plain truncation comes at a cost in closure. In general, the unitary Hausdorff series does not terminate, so a finite excitation space cannot close under

it, in contrast to the terminating expansion of standard similarity-transformed CC. The commutators $[\hat{\Xi}_{0,\mu}, \hat{\Xi}_{0,\nu}]$ can create outside terms. The similarity transform $\tilde{B}_y(t) = e^{-\hat{y}}\hat{B}e^{\hat{y}}$ can leak out of the manifold and let the surviving cumulants pick up nonlocal contributions; and the Jacobi argument for the symmetric Jacobian fails, so $\mathbf{A}$ would have to be symmetrized by hand.

Closing only the $\mathrm{ad}_{\hat{y}}$ component of $\hat{B}$ makes $\tilde{B}_y$ well-behaved while the trajectory $\hat{y}(t)$ stays approximate in nature. For a target dimension M, completing the manifold to a closed $\mathfrak{su}(M)$ puts the propagation on the invariant subspace $\mathcal{H}_M$ that the algebra generates, leaving the Hamiltonian coupling between $\mathcal{H}_M$ and its complement. The FCI limit (dimension N) is the maximal case $\mathcal{H}_N = \mathcal{H}$, where this coupling vanishes. A closed $\mathfrak{su}(M)$ need not be local, so additivity for separated subsystems requires the completion to feature locality; otherwise small nonlocality leaks remain, as in truncated EOM-CC and ic-MRCC. The piecewise restarts bound amplitude growth without restoring closure. In addition, applications will have to take supermolecular additivity into account.

The Dirac-Frenkel strategy followed in this work is shared with the multiconfiguration time-dependent Hartree method, tensor-network TDVP schemes, and variational quantum simulation [137–139]. Our working equation, $\sum_\nu \mathrm{Im}[S'_{\mu\nu}(t)]\dot{y}_{\mathrm{i},\nu} = -\mathrm{Re}[h_{\mathrm{eff},\mu}(t)]$, has the form of a metric acting on "rates". Some differences: the real/imaginary split follows from the anti-Hermitian generator, while the metric and the $\hat{\Xi}_{\mathrm{I},\mu}$ operators come from the internally contracted cluster algebra after SVD orthogonalization and QR rotation. Both could serve as a starting point for further work on unitary TD theories and their numerics.

5 Conclusion

We have presented a time-dependent unitary coupled-cluster approach to the propagation of general quantum states. A time-dependent anti-Hermitian cluster operator generates the non-ground-state wave function component, while the evolution is unitary, and norms are conserved. The observables are strictly real-valued. Variations of the Dirac-Frenkel action give equations of motion expressed through Heisenberg-like commutators. The unperturbed dynamics yields the EOM-UCC eigenvalue problem, which is based on a symmetric Jacobian. For the free propagation of general initial states, the observable expressions can be linked, with the unphysical vacuum factor cancelling against the normalization. Size-extensivity, however, must be considered in detail as EOM methods are still subject to unwanted non-localities. The numerical tests reproduced the reference dipoles, populations, and coherences, while the piecewise restarts kept long propagations stable. The correlation function is not exact in the present formulation; treating it, and applying the theory to realistic atomic and molecular systems, are potential future steps.

Funding

This material is based upon work supported by the U.S. Department of Energy, Office of Science, Office of Basic Energy Sciences, Early Career Research Program, Award Number DE-SC-0025662.

Author contributions

Martín A. Mosquera: Conceptualization, Methodology, Software, Formal analysis, Investigation, Writing – original draft, Writing – review and editing.

Data availability

The data that support the findings of this study are openly available at the following URL/DOI: https://doi.org/10.5281/zenodo.22017136. The deposit contains the simulation code, the input files, and the propagation and eigenvalue output underlying every figure and table in this article and in the supplementary material. It is released under a CC BY 4.0 licence.

Supplementary data

The supplementary material is appended to this preprint (Secs. S1–S5). Derivation of the Maurer-Cartan relation and the first-order generator equation of motion, linked observable expressions, observable matrix elements and their supermolecular additivity, and results for truncated excitation spaces including the active space and CAS-CI eigenvectors, ground-state and excitation energies, converged cluster amplitudes, and the first EOM-UCC excitation vector.

References

[1] Krausz F and Ivanov M 2014 *Rev. Mod. Phys.* **86** 153

[2] Lépine F, Ivanov M Y and Vrakking M J J 2014 *Nat. Photon.* **8** 195–204

[3] Nisoli M, Decleva P and Calegari F 2017 *Chem. Rev.* **117** 10760–10825

[4] Palacios A and Martín F 2020 *WIREs Comput. Mol. Sci.* **10** e1430

[5] Nelson T R, White A J, Bjorgaard J A, Sifain A E, Zhang Y, Nebgen B, Fernandez-Alberti S, Mozyrsky D, Roitberg A E and Tretiak S 2020 *Chem. Rev.* **120** 2215–2287

[6] Matsika S 2021 *Chem. Rev.* **121** 9407–9449

[7] Casida M E and Huix-Rotllant M 2012 *Annu. Rev. Phys. Chem.* **63** 287–323

[8] Mosquera M A and Wasserman A 2015 *J. Chem. Theory Comput.* **11** 3530–3536

[9] Kirrander A and Vacher M 2020 *Quantum Chemistry and Dynamics of Excited States: Methods and Applications* 469–497

[10] Fernandez-Alberti S, Makhov D V, Tretiak S and Shalashilin D V 2016 *Phys. Chem. Chem. Phys.* **18** 10028–10040

[11] Li X, Tully J C, Schlegel H B and Frisch M J 2005 *J. Chem. Phys.* **123**

[12] Mosquera M A, Chen L X, Ratner M A and Schatz G C 2016 *J. Chem. Phys.* **144** 204105

[13] Kjaergaard M, Schwartz M E, Braumüller J, Krantz P, Wang J I J, Gustavsson S and Oliver W D 2020 *Annu. Rev. Condens. Matter Phys.* **11** 369–395

[14] Flamini F, Spagnolo N and Sciarrino F 2018 *Rep. Prog. Phys.* **82** 016001

[15] Bruzewicz C D, Chiaverini J, McConnell R and Sage J M 2019 *Appl. Phys. Rev.* **6**

[16] Wang J, Sciarrino F, Laing A and Thompson M G 2020 *Nat. Photonics* **14** 273–284

[17] Saffman M 2016 *J. Phys. B: At. Mol. Opt. Phys.* **49** 202001

[18] Bernien H, Schwartz S, Keesling A, Levine H, Omran A, Pichler H, Choi S, Zibrov A S, Endres M, Greiner M *et al.* 2017 *Nature* **551** 579–584

[19] Browaeys A and Lahaye T 2020 *Nat. Physics* **16** 132–142

[20] Bluvstein D, Levine H, Semeghini G, Wang T T, Ebadi S, Kalinowski M, Keesling A, Maskara N, Pichler H, Greiner M *et al.* 2022 *Nature* **604** 451–456

[21] Henriet L, Beguin L, Signoles A, Lahaye T, Browaeys A, Reymond G O and Jurczak C 2020 *Quantum* **4** 327

[22] Weiss D S and Saffman M 2017 *Phys. Today* **70** 44–50

[23] Wurtz J, Bylinskii A, Braverman B, Amato-Grill J, Cantu S H, Huber F, Lukin A, Liu F, Weinberg P, Long J *et al.* 2023 *arXiv preprint arXiv:2306.11727*

[24] Brennen G K, Caves C M, Jessen P S and Deutsch I H 1999 *Phys. Rev. Lett.* **82** 1060

[25] Jaksch D, Briegel H J, Cirac J, Gardiner C and Zoller P 1999 *Phys. Rev. Lett.* **82** 1975

[26] Jaksch D, Cirac J I, Zoller P, Rolston S L, Côté R and Lukin M D 2000 *Phys. Rev. Lett.* **85** 2208

[27] Ahn J, Weinacht T and Bucksbaum P 2000 *Science* **287** 463–465

[28] Omran A, Levine H, Keesling A, Semeghini G, Wang T T, Ebadi S, Bernien H, Zibrov A S, Pichler H, Choi S *et al.* 2019 *Science* **365** 570–574

[29] Gross C and Bloch I 2017 *Science* **357** 995–1001

[30] Evered S J, Bluvstein D, Kalinowski M, Ebadi S, Manovitz T, Zhou H, Li S H, Geim A A, Wang T T, Maskara N *et al.* 2023 *Nature* **622** 268–272

[31] Saffman M 2019 *Natl. Sci. Rev.* **6** 24–25

[32] Levine H, Keesling A, Omran A, Bernien H, Schwartz S, Zibrov A S, Endres M, Greiner M, Vuletić V and Lukin M D 2018 *Phys. Rev. Lett.* **121** 123603

[33] Graham T, Kwon M, Grinkemeyer B, Marra Z, Jiang X, Lichtman M, Sun Y, Ebert M and Saffman M 2019 *Phys. Rev. Lett.* **123** 230501

[34] Saffman M, Walker T G and Mølmer K 2010 *Rev. Mod. Phys.* **82** 2313

[35] Saffman M and Mølmer K 2008 *Phys. Rev. A* **78** 012336

[36] Ates C, Pohl T, Pattard T and Rost J M 2007 *Phys. Rev. A* **76** 013413

[37] Graham T, Song Y, Scott J, Poole C, Phuttitarn L, Jooya K, Eichler P, Jiang X, Marra A, Grinkemeyer B *et al.* 2022 *Nature* **604** 457–462

[38] Čížek J 1966 *J. Chem. Phys.* **45** 4256–4266

[39] Bartlett R J and Musiał M 2007 *Rev. Mod. Phys.* **79** 291–352

[40] Paldus J 1994 Algebraic approach to coupled cluster theory *Relativistic and Electron Correlation Effects in Molecules and Solids* ed Malli G L (Boston, MA: Springer US) pp 207–282

[41] Čížek J 1969 *Adv. Chem. Phys.* **14** 35–89

[42] Shavitt I 1998 *Mol. Phys.* **94** 3–17

[43] Bartlett R J and Purvis G D 1978 *Int. J. Quantum Chem.* **14** 561–581

[44] Helgaker T, Jørgensen P and Olsen J 2014 *Molecular electronic-structure theory* (John Wiley & Sons)

[45] Nakatsuji H 1978 *Chem. Phys. Lett.* **59** 362–364

[46] Nakatsuji H 1979 *Chem. Phys. Lett.* **67** 329–333

[47] Monkhorst H J 1977 *Int. J. Quantum Chem.* **12** 421–432

[48] Koch H and Jørgensen P 1990 *J. Chem. Phys.* **93** 3333–3344

[49] Christiansen O, Jørgensen P and Hättig C 1998 *International Journal of Quantum Chemistry* **68** 1–52

[50] Stanton J F and Bartlett R J 1993 *J. Chem. Phys.* **98** 7029–7039

[51] Krylov A I 2008 *Annu. Rev. Phys. Chem.* **59** 433–462

[52] Bartlett R J 2012 *WIREs Comput. Mol. Sci.* **2** 126–138

[53] Sneskov K and Christiansen O 2012 *WIREs Comput. Mol. Sci.* **2** 566–584

[54] Koch H and Harrison R J 1991 *J. Chem. Phys.* **95** 7479–7485

[55] Pedersen T B and Koch H 1997 *J. Chem. Phys.* **106** 8059–8072

[56] Nascimento D R and DePrince III A E 2019 *J. Chem. Phys.* **151** 204107

[57] Mukherjee D and Pal S 1989 *Adv. Quantum Chem.* **20** 291–373

[58] Evangelista F A 2018 *J. Chem. Phys.* **149** 030901

[59] Jeziorski B 2010 *Mol. Phys.* **108** 3043–3054

[60] Mahapatra U S, Datta B and Mukherjee D 1998 *Mol. Phys.* **94** 157–171

[61] Mahapatra U S, Datta B and Mukherjee D 1999 *J. Chem. Phys.* **110** 6171–6188

[62] Evangelista F A and Gauss J 2011 *J. Chem. Phys.* **134**

[63] Hanauer M and Köhn A 2012 *J. Chem. Phys.* **137**

[64] Hanrath M 2005 *J. Chem. Phys.* **123**

[65] Hanrath M 2008 *Mol. Phys.* **106** 1949–1957

[66] Datta D and Nooijen M 2012 *J. Chem. Phys.* **137**

[67] Park J W, Al-Saadon R, MacLeod M K, Shiozaki T and Vlaisavljevich B 2020 *Chem. Rev.* **120** 5878–5909

[68] Maitra R, Sinha D and Mukherjee D 2012 *J. Chem. Phys.* **137** 024105

[69] Köhn A, Hanauer M, Mueck L A, Jagau T C and Gauss J 2013 *WIREs Comput. Mol. Sci.* **3** 176–197

[70] Chattopadhyay S, Mahapatra U S and Mukherjee D 2000 *J. Chem. Phys.* **112** 7939–7952

[71] Samanta P K, Mukherjee D, Hanauer M and Köhn A 2014 *J. Chem. Phys.* **140** 134108

[72] Jagau T C and Gauss J 2012 *J. Chem. Phys.* **137** 044116

[73] Lechner M H, Izsák R, Nooijen M and Neese F 2021 *Mol. Phys.* **119** e1939185

[74] Hirata S 2026 *J. Chem. Phys.* **165** 064113

[75] Arponen J 1983 *Ann. Phys.–New York* **151** 311–382

[76] Dalgaard E and Monkhorst H J 1983 *Phys. Rev. A* **28** 1217

[77] Kvaal S 2012 *J. Chem. Phys.* **136** 194109

[78] Pedersen T B and Kvaal S 2019 *J. Chem. Phys.* **150** 144106

[79] Sato T, Pathak H, Orimo Y and Ishikawa K L 2018 *J. Chem. Phys.* **148** 051101

[80] Skeidsvoll A S, Balbi A and Koch H 2020 *Phys. Rev. A* **102** 023115

[81] Skeidsvoll A S, Moitra T, Balbi A, Paul A C, Coriani S and Koch H 2022 *Phys. Rev. A* **105** 023103

[82] White A F and Chan G K L 2018 *J. Chem. Theory Comput.* **14** 5690–5700

[83] White A F and Chan G K L 2019 *J. Chem. Theory Comput.* **15** 6137–6153

[84] Pathak H, Sato T and Ishikawa K L 2021 *J. Chem. Phys.* **154** 234104

[85] Pathak H, Sato T and Ishikawa K L 2022 *Front. Chem.* **10** 982120

[86] Koulias L N, Williams-Young D B, Nascimento D R, DePrince III A E and Li X 2019 *J. Chem. Theory Comput.* **15** 6617–6624

[87] Wang Z, Peyton B G and Crawford T D 2022 *J. Chem. Theory Comput.* **18** 5479–5491

[88] Ofstad B S, Aurbakken E, Schøyen Ø S, Kristiansen H E, Kvaal S and Pedersen T B 2023 *WIREs Comput. Mol. Sci.* e1666

[89] Pedersen T B and Koch H 1998 *J. Chem. Phys.* **108** 5194–5204

[90] Pedersen T B, Kristiansen H E, Bodenstein T, Kvaal S and Schøyen Ø S 2020 *J. Chem. Theory Comput.* **17** 388–404

[91] Pigg D A, Hagen G, Nam H and Papenbrock T 2012 *Phys. Rev. C* **86** 014308

[92] Hoodbhoy P and Negele J 1978 *Phys. Rev. C* **18** 2380

[93] Hoodbhoy P and Negele J 1979 *Phys. Rev. C* **19** 1971

[94] Schönhammer K and Gunnarsson O 1978 *Phys. Rev. B* **18** 6606

[95] Guha S and Mukherjee D 1991 *Chem. Phys. Lett.* **186** 84–90

[96] Nascimento D R and DePrince III A E 2016 *J. Chem. Theor. Comput.* **12** 5834–5840

[97] Nascimento D R and DePrince III A E 2017 *J. Phys. Chem. Lett.* **8** 2951–2957

[98] Harsha G, Shiozaki T and Scuseria G E 2018 *J. Chem. Phys.* **148** 044107

[99] Kats D, Usvyat D and Schütz M 2011 *Phys. Rev. A* **83** 062503

[100] Wälz G, Kats D, Usvyat D, Korona T and Schütz M 2012 *Phys. Rev. A* **86** 052519

[101] Kutzelnigg W 1977 Pair correlation theories *Methods of electronic structure theory* (Springer) pp 129–188

[102] Prasad M D, Pal S and Mukherjee D 1985 *Phys. Rev. A* **31** 1287

[103] Bartlett R J, Kucharski S A and Noga J 1989 *Chem. Phys. Lett.* **155** 133–140

[104] Kutzelnigg W 1991 *Theor. Chim. Acta* **80** 349–386

[105] Taube A G and Bartlett R J 2006 *Int. J. Quantum Chem.* **106** 3393–3401

[106] Liu J, Asthana A, Cheng L and Mukherjee D 2018 *The Journal of chemical physics* **148** 244110

[107] Hodecker M and Dreuw A 2020 *The Journal of Chemical Physics* **153**

[108] Cao Y, Romero J, Olson J P, Degroote M, Johnson P D, Kieferová M, Kivlichan I D, Menke T, Peropadre B, Sawaya N P *et al.* 2019 *Chem. Rev.* **119** 10856–10915

[109] McArdle S, Endo S, Aspuru-Guzik A, Benjamin S C and Yuan X 2020 *Rev. Mod. Phys.* **92** 015003

[110] Bauer B, Bravyi S, Motta M and Chan G K L 2020 *Chem. Rev.* **120** 12685–12717

[111] Motta M and Rice J E 2022 *WIREs Comput. Mol. Sci.* **12** e1580

[112] Ryabinkin I G, Yen T C, Genin S N and Izmaylov A F 2018 *J. Chem. Theory Comput.* **14** 6317–6326

[113] Romero J, Babbush R, McClean J R, Hempel C, Love P J and Aspuru-Guzik A 2018 *Quantum Sci. Technol.* **4** 014008

[114] Xia R and Kais S 2020 *Quantum Sci. Technol.* **6** 015001

[115] Tilly J, Jones G, Chen H, Wossnig L and Grant E 2020 *Phys. Rev. A* **102** 062425

[116] Anand A, Schleich P, Alperin-Lea S, Jensen P W, Sim S, Díaz-Tinoco M, Kottmann J S, Degroote M, Izmaylov A F and Aspuru-Guzik A 2022 *Chem. Soc. Rev.* **51** 1659–1684

[117] Shen Y, Zhang X, Zhang S, Zhang J N, Yung M H and Kim K 2017 *Phys. Rev. A* **95** 020501

[118] Lee J, Huggins W J, Head-Gordon M and Whaley K B 2018 *J. Chem. Theory Comput.* **15** 311–324

[119] Evangelista F A, Chan G K and Scuseria G E 2019 *J. Chem. Phys.* **151** 244112

[120] Higgott O, Wang D and Brierley S 2019 *Quantum* **3** 156

[121] Sokolov I O, Barkoutsos P K, Ollitrault P J, Greenberg D, Rice J, Pistoia M and Tavernelli I 2020 *The Journal of chemical physics* **152** 124107

[122] Cervia M J, Balantekin A, Coppersmith S, Johnson C W, Love P J, Poole C, Robbins K and Saffman M 2021 *Phys. Rev. C* **104** 024305

[123] Smith J S, Nebgen B T, Zubatyuk R, Lubbers N, Devereux C, Barros K, Tretiak S, Isayev O and Roitberg A E 2019 *Nat. Commun.* **10** 1–8

[124] Fleury A, Brown J, Lloyd E, Hernandez M and Kim I H 2024 *J. Chem. Theory Comput.* **20** 10807–10816

[125] Kim Y and Krylov A I 2023 *J. Phys. Chem. A* **127** 6552–6566

[126] Datta D and Gauss J 2013 *J. Chem. Theory Comput.* **9** 2639–2653

[127] Li S, Zhao Z and Evangelista F A 2025 *J. Chem. Phys.* **162** 154112

[128] Bauman N P, Bylaska E J, Krishnamoorthy S, Low G H, Wiebe N, Granade C E, Roetteler M, Troyer M and Kowalski K 2019 *J. Chem. Phys.* **151** 014107

[129] Kowalski K and Bauman N P 2020 *J. Chem. Phys.* **152** 244127

[130] Mosquera M A 2022 *Phys. Rev. A* **106** 052805

[131] Mosquera M A, Jones L O, Kang G, Ratner M A and Schatz G C 2021 *J. Phys. Chem. A* **125** 1093–1102

[132] Mosquera M A 2023 *Electron. Struct.* **5** 045001

[133] Mosquera M A 2025 *Phys. Rev. A* **112** 012825

[134] Rowe D J 1968 *Rev. Mod. Phys.* **40** 153–166

[135] Kutzelnigg W and Mukherjee D 1997 *J. Chem. Phys.* **107** 432–449

[136] Mukherjee D 1997 *Chem. Phys. Lett.* **274** 561–566

[137] Li Y and Benjamin S C 2017 *Phys. Rev. X* **7** 021050

[138] Yuan X, Endo S, Zhao Q, Li Y and Benjamin S C 2019 *Quantum* **3** 191

[139] McArdle S, Jones T, Endo S, Li Y, Benjamin S C and Yuan X 2019 *npj Quantum Inf.* **5** 75

Supplementary material: Observables and anti-Hermitian generators in time-dependent unitary coupled cluster theory

Martín A. Mosquera

Department of Chemistry and Biochemistry, Montana State University, Bozeman, Montana 59717, USA

S1 Maurer-Cartan Relation

Here we derive the variations $\hat{\Xi}_\mu^{(n)}(t)$ and the first-order residual $\hat{R}^{(1)}(t)$ used in the main text. Both follow from derivatives of the exponential map $\hat{U}_\mathrm{m} = \exp[\hat{x}_\mathrm{m}(t;g)]$ in the continuous parameter g, evaluated at $g = 0$.

The residual is $\hat{R}_\mathrm{m}(t;g) = \mathrm{i}\,\hat{\pi}_{x_\mathrm{m}}(\partial_t \hat{x}_\mathrm{m}) - \hat{H}_{x_\mathrm{m}}$, with the transformed Hamiltonian $\hat{H}_{x_\mathrm{m}} = e^{-\hat{x}_\mathrm{m}} \hat{H} e^{\hat{x}_\mathrm{m}}$ and the transformed basis operator $\hat{\Xi}_{\mathrm{m},\mu}(t;g) = \hat{\pi}_{x_\mathrm{m}}(\hat{\kappa}_\mu)$. The continuous generator is $\tilde{z}(t;g) = \hat{\pi}_{x_\mathrm{m}}(\partial_g \hat{x}_\mathrm{m})$. We use the Maurer-Cartan relation for the projection map [Eq. (3) of Ref. [133]]:

$$\partial_\alpha(\hat{\pi}_u(\partial_\beta \hat{u})) - \partial_\beta(\hat{\pi}_u(\partial_\alpha \hat{u})) = [\hat{\pi}_u(\partial_\beta \hat{u}), \hat{\pi}_u(\partial_\alpha \hat{u})] \; . \tag{S1}$$

Setting $\hat{u} = \hat{x}_\mathrm{m}$, $\beta = g$, and $\alpha = x_{\mathrm{m},\mu}$ gives $\hat{\pi}_u(\partial_\beta \hat{u}) = \tilde{z}(t;g)$ and $\hat{\pi}_u(\partial_\alpha \hat{u}) = \hat{\Xi}_{\mathrm{m},\mu}$, so

$$\partial_g \hat{\Xi}_{\mathrm{m},\mu} = \partial_\mu \tilde{z}(t;g) + [\hat{\Xi}_{\mathrm{m},\mu}, \tilde{z}(t;g)] \; . \tag{S2}$$

Evaluated at $g = 0$, this yields the first-order variation

$$\hat{\Xi}_\mu^{(1)}(t) = \partial_\mu \tilde{z}(t) + [\hat{\Xi}_\mu^{(0)}(t), \tilde{z}(t)] \; , \qquad \hat{\Xi}_\mu^{(0)}(t) = \hat{\pi}_x(\hat{\kappa}_\mu) \; , \tag{S3}$$

in agreement with the main text.

Taking instead $\alpha = t$ and $\beta = g$ gives

$$\partial_g \left[\hat{\pi}_{x_\mathrm{m}}(\partial_t \hat{x}_\mathrm{m})\right] = \partial_t \tilde{z}(t;g) + [\hat{\pi}_{x_\mathrm{m}}(\partial_t \hat{x}_\mathrm{m}), \tilde{z}(t;g)] \; , \tag{S4}$$

and, since the transformed Hamiltonian is a similarity transform of a fixed operator, its derivative is the commutator

$$\partial_g \hat{H}_{x_\mathrm{m}} = [\hat{H}_{x_\mathrm{m}}, \tilde{z}(t;g)] \; . \tag{S5}$$

Combining the last two relations, the derivative of the residual is

$$\partial_g \hat{R}_\mathrm{m} = \mathrm{i}\,\partial_g \left[\hat{\pi}_{x_\mathrm{m}}(\partial_t \hat{x}_\mathrm{m})\right] - \partial_g \hat{H}_{x_\mathrm{m}} = \mathrm{i}\,\partial_t \tilde{z}(t;g) + [\hat{R}_\mathrm{m}, \tilde{z}(t;g)] \; . \tag{S6}$$

Evaluated at $g = 0$, with $\tilde{z}(t) = \tilde{z}(t;g)\big|_{g=0}$ and $\hat{R}_x = \hat{R}_\mathrm{m}\big|_{g=0}$, this gives

$$\hat{R}^{(1)}(t) = \mathrm{i}\,\partial_t \tilde{z}(t) + [\hat{R}_x(t), \tilde{z}(t)] \; , \tag{S7}$$

which is the first-order residual quoted in the main text.

S2 First-Order Generator Equation of Motion

The generator $\tilde{z}(t)$ obeys an equation of motion obtained by differentiating the propagation condition

$$\langle [\hat{\Xi}_{\mathrm{m},\mu}(t;g) \, , \, \hat{R}_\mathrm{m}(t;g)] \rangle = 0 \tag{S8}$$

with respect to g and evaluating at $g = 0$. With $\hat{\Xi}_{\mathrm{m},\mu}\big|_{g=0} = \hat{\Xi}^{(0)}_{\mu}(t)$, $\partial_g \hat{\Xi}_{\mathrm{m},\mu}\big|_{g=0} = \hat{\Xi}^{(1)}_{\mu}(t)$, $\hat{R}_{\mathrm{m}}\big|_{g=0} = \hat{R}_x(t)$, and $\partial_g \hat{R}_{\mathrm{m}}\big|_{g=0} = \hat{R}^{(1)}(t)$, this gives

$$\langle [\hat{\Xi}^{(1)}_{\mu}(t)\,,\,\hat{R}_x(t)]\rangle + \langle [\hat{\Xi}^{(0)}_{\mu}(t)\,,\,\hat{R}^{(1)}(t)]\rangle = 0\ . \tag{S9}$$

Substituting the first-order residual $\hat{R}^{(1)}(t) = \mathrm{i}\partial_t \tilde{z}(t) + [\hat{R}_x(t), \tilde{z}(t)]$ from Sec. S1 and isolating the time derivative,

$$\langle [\hat{\Xi}^{(0)}_{\mu}(t)\,,\,\mathrm{i}\partial_t \tilde{z}(t)]\rangle = -\langle [\hat{\Xi}^{(0)}_{\mu}(t)\,,\,[\hat{R}_x(t), \tilde{z}(t)]]\rangle - \langle [\hat{\Xi}^{(1)}_{\mu}(t)\,,\,\hat{R}_x(t)]\rangle\ . \tag{S10}$$

This is the working equation for the first-order generator shown in the main text. It applies to both free and driven propagation and is accurate at short times. The reference operator $\hat{x}(t)$ carries the nonlinear part of the evolution, while $\tilde{z}(t)$ tracks the linear response.

S3 Linked Observable Expressions

Let the reference be $|\bar{\Psi}(0)\rangle = [c_0 + \tilde{z}(0)]|0\rangle$, with $\tilde{z}(0)$ anti-Hermitian ($\tilde{z}^\dagger(0) = -\tilde{z}(0)$), and let $\tilde{B}_y(t) = \hat{U}_y^\dagger(t)\hat{B}\hat{U}_y(t)$. The expectation value is

$$\langle \hat{B}\rangle(t) = \frac{\langle [c_0^* - \tilde{z}(0)]\tilde{B}_y(t)[c_0 + \tilde{z}(0)]\rangle}{|c_0|^2 + \langle -\tilde{z}^2(0)\rangle}\ . \tag{S11}$$

The denominator $D \equiv |c_0|^2 + \langle -\tilde{z}^2(0)\rangle$ is the squared norm $\langle \bar{\Psi}(0)|\bar{\Psi}(0)\rangle$; its linear cross terms vanish because $\langle \tilde{z}(0)\rangle = 0$, enforced by the reference-component convention adopted in the main text. Each eigenvector satisfies $\langle \tilde{X}^I\rangle = 0$, which each commutator of the working equations ignores.

Expanding the numerator gives

$$\begin{aligned}\langle [c_0^* - \tilde{z}(0)]\tilde{B}_y(t)[c_0 + \tilde{z}(0)]\rangle = |c_0|^2\langle \tilde{B}_y(t)\rangle + c_0^*\langle \tilde{B}_y(t)\tilde{z}(0)\rangle \\ - c_0\langle \tilde{z}(0)\tilde{B}_y(t)\rangle - \langle \tilde{z}(0)\tilde{B}_y(t)\tilde{z}(0)\rangle\ .\end{aligned} \tag{S12}$$

The quadratic term has the same operator on both sides, so it splits into a double commutator and an anticommutator,

$$-\langle \tilde{z}(0)\tilde{B}_y(t)\tilde{z}(0)\rangle = \frac{1}{2}\langle [[\tilde{B}_y(t), \tilde{z}(0)], \tilde{z}(0)]\rangle - \frac{1}{2}\langle \{\tilde{B}_y(t), \tilde{z}^2(0)\}\rangle\ . \tag{S13}$$

Wick's theorem separates the anticommutator into disconnected and connected parts,

$$-\frac{1}{2}\langle \{\tilde{B}_y(t), \tilde{z}^2(0)\}\rangle = -\langle \tilde{B}_y(t)\rangle\langle \tilde{z}^2(0)\rangle - \frac{1}{2}\langle \{\tilde{B}_y(t), \tilde{z}^2(0)\}\rangle_{\mathrm{C}}\ , \tag{S14}$$

where the subscript C denotes the connected contribution. The disconnected piece combines with the leading term,

$$|c_0|^2\langle \tilde{B}_y(t)\rangle - \langle \tilde{B}_y(t)\rangle\langle \tilde{z}^2(0)\rangle = \langle \tilde{B}_y(t)\rangle\left(|c_0|^2 - \langle \tilde{z}^2(0)\rangle\right) = D\langle \tilde{B}_y(t)\rangle\ , \tag{S15}$$

so dividing by D removes it and leaves $\langle \tilde{B}_y(t)\rangle$. The observable becomes

$$\begin{aligned}\langle \hat{B}\rangle(t) = \langle \tilde{B}_y(t)\rangle + \frac{1}{D}\Big(c_0^*\langle \tilde{B}_y(t)\tilde{z}(0)\rangle - c_0\langle \tilde{z}(0)\tilde{B}_y(t)\rangle \\ + \frac{1}{2}\langle [[\tilde{B}_y(t), \tilde{z}(0)], \tilde{z}(0)]\rangle - \frac{1}{2}\langle \{\tilde{B}_y(t), \tilde{z}^2(0)\}\rangle_{\mathrm{C}}\Big)\ ,\end{aligned} \tag{S16}$$

which is the size-extensive form used in the main text. The disconnected vacuum factor, the product of $\langle \tilde{B}_y(t)\rangle$ and $\langle \tilde{z}^2(0)\rangle$, has cancelled against the normalization.

S4 Observable Matrix Elements

The observable of Sec. S3 is quadratic in $\tilde{z}(0)$, where initial conditions can reveal matrix elements between EOM-UCC states in the same linked form, with no additional requirements. We derive the expressions here.

The relevant operator is the transformed object:

$$\tilde{B}_T \equiv e^{-\hat{T}} \hat{B} e^{\hat{T}} \ . \tag{S17}$$

The correlated states are $|\Psi_K\rangle = e^{\hat{T}} \tilde{X}^K |0\rangle$ ($|\Psi_0\rangle = e^{\hat{T}}|0\rangle$). Since $\hat{T}$ is anti-Hermitian, $e^{\hat{T}\dagger} = e^{-\hat{T}}$, and we have that $\langle \Psi_I | \hat{B} | \Psi_J \rangle = \langle \Phi_I | \tilde{B}_T | \Phi_J \rangle$ with $|\Phi_K\rangle = \tilde{X}^K |0\rangle$.

We denote $\langle \cdot \rangle \equiv \langle 0| \cdot |0\rangle$, and assume the condition $\tilde{X}^{K\dagger}|0\rangle = 0$, equivalently $\langle 0 | \tilde{X}^K = 0$. This condition holds in the FCI limit or closed-algebra cases. Taking the adjoint of the eigenrelation $[\hat{H}_T, \tilde{X}^K] = \Omega_K \tilde{X}^K$ gives $[\hat{H}_T, \tilde{X}^{K\dagger}] = -\Omega_K \tilde{X}^{K\dagger}$. Applying this to the reference, with $\hat{H}_T|0\rangle = E_0|0\rangle$ in the same limit, yields

$$\hat{H}_T \left(\tilde{X}^{K\dagger}|0\rangle \right) = (E_0 - \Omega_K) \left(\tilde{X}^{K\dagger}|0\rangle \right) \ , \tag{S18}$$

which demands that $\tilde{X}^{K\dagger}|0\rangle = 0$. In general, under truncations/approximations the relations derived next, and the annihilating condition, hold only approximately, but these become exact in the FCI limit, or closed-algebraic systems. We now write

$$\delta \tilde{B}_T \equiv \tilde{B}_T - \langle \tilde{B}_T \rangle \tag{S19}$$

for the fluctuation operator, and $S_{IJ} \equiv \langle \Phi_I | \Phi_J \rangle$ for the overlap between eigenstates.

The initial generator $\tilde{z}(0) = \sum_{I>0} (c_I \tilde{X}^I - c_I^* \tilde{X}^{I\dagger})$ admits complex coefficients. The two phase choices $c_K = 1$ and $c_K = \mathrm{i}$ produce the anti-Hermitian pair

$$z_K = \tilde{X}^K - \tilde{X}^{K\dagger} \ , \qquad w_K = \mathrm{i} \left(\tilde{X}^K + \tilde{X}^{K\dagger} \right) \ , \tag{S20}$$

whose action on the reference follows from the annihilating condition,

$$z_K|0\rangle = |\Phi_K\rangle \ , \quad \langle 0|z_K = -\langle \Phi_K| \ , \qquad w_K|0\rangle = \mathrm{i}|\Phi_K\rangle \ , \quad \langle 0|w_K = +\mathrm{i}\langle \Phi_K| \ . \tag{S21}$$

The relative sign between bra and ket is negative for z_K and positive for w_K. This single asymmetry is what separates the real and imaginary parts below.

Let a and b be any two anti-Hermitian operators. Expanding both orderings of the double commutator, we get:

$$\langle [[\tilde{B}_T, a], b] \rangle = \langle \tilde{B}_T ab \rangle - \langle a \tilde{B}_T b \rangle - \langle b \tilde{B}_T a \rangle + \langle ba \tilde{B}_T \rangle \ , \tag{S22}$$

$$\langle [[\tilde{B}_T, b], a] \rangle = \langle \tilde{B}_T ba \rangle - \langle b \tilde{B}_T a \rangle - \langle a \tilde{B}_T b \rangle + \langle ab \tilde{B}_T \rangle \ . \tag{S23}$$

We can also note that

$$\langle [[\tilde{B}_T, a], b] \rangle + \langle [[\tilde{B}_T, b], a] \rangle = \langle \{ \tilde{B}_T, \{a, b\} \} \rangle - 2 \left(\langle a \tilde{B}_T b \rangle + \langle b \tilde{B}_T a \rangle \right) \ . \tag{S24}$$

The anticommutator above is not linked. It contains the disconnected piece $2\langle \tilde{B}_T \rangle \langle \{a, b\} \rangle$. We therefore define the bilinear functional with its connected part, in the same convention as Sec. S3,

$$\begin{aligned} F_{\mathrm{C}}[a, b] &\equiv \frac{1}{2} \left(\langle [[\tilde{B}_T, a], b] \rangle + \langle [[\tilde{B}_T, b], a] \rangle \right) - \frac{1}{2} \langle \{ \tilde{B}_T, \{a, b\} \} \rangle_{\mathrm{C}} \ , \\ \langle \{ \tilde{B}_T, W \} \rangle_{\mathrm{C}} &= \langle \{ \tilde{B}_T, W \} \rangle - 2 \langle \tilde{B}_T \rangle \langle W \rangle \ . \end{aligned} \tag{S25}$$

Combining Eqs. (S24) and (S25) gives the compact evaluation

$$F_{\mathrm{C}}[a,b] = -\Big(\langle a\,\delta\tilde{B}_T\,b\rangle + \langle b\,\delta\tilde{B}_T\,a\rangle\Big)\ , \tag{S26}$$

that is, the plain result with $\tilde{B}_T$ replaced by the fluctuation operator of Eq. (S19). This form makes the linkedness explicit. Since $\langle a\rangle = \langle b\rangle = 0$, the generalized Wick contraction over the correlated reference, discussed in the main text, reduces $\langle a\,\delta\tilde{B}_T\,b\rangle$. The invariance of all terms of Eq. (S25) under $\hat{B} \to \hat{B} + c$ is a check of this reduction, but not a proof of linkedness. Setting $a = b = \tilde{z}(0)$ recovers the quadratic term of Sec. S3: $F_{\mathrm{C}}[\tilde{z}(0),\tilde{z}(0)] = -2\langle\tilde{z}(0)\,\delta\tilde{B}_T\,\tilde{z}(0)\rangle$, which is twice the combination that Eq. (S16) is left with once the disconnected vacuum factor has cancelled against the normalization.

S4.1 Real and imaginary parts

Taking $a = z_I$ and $b = z_J$ in Eq. (S26) and inserting Eq. (S21), the two sign flips multiply to $+1$,

$$F_{\mathrm{C}}[z_I,z_J] = \langle\Phi_I|\delta\tilde{B}_T|\Phi_J\rangle + \langle\Phi_J|\delta\tilde{B}_T|\Phi_I\rangle = 2\,\mathrm{Re}\,\langle\Phi_I|\delta\tilde{B}_T|\Phi_J\rangle\ , \tag{S27}$$

the last step using the Hermiticity of $\hat{B}$. Taking instead $a = z_I$ and $b = w_J$, only one sign flips, and the two terms subtract rather than add,

$$F_{\mathrm{C}}[z_I,w_J] = \mathrm{i}\Big(\langle\Phi_I|\delta\tilde{B}_T|\Phi_J\rangle - \langle\Phi_J|\delta\tilde{B}_T|\Phi_I\rangle\Big) = -2\,\mathrm{Im}\,\langle\Phi_I|\delta\tilde{B}_T|\Phi_J\rangle\ . \tag{S28}$$

Combining the two last results gives the complex transition moment in linked form,

$$\langle\Phi_I|\tilde{B}_T|\Phi_J\rangle - \langle\tilde{B}_T\rangle S_{IJ} = \frac{1}{2}F_{\mathrm{C}}[z_I,z_J] - \frac{\mathrm{i}}{2}F_{\mathrm{C}}[z_I,w_J] \tag{S29}$$

Every term on the right is a commutator or a connected anticommutator of $\tilde{B}_T$ with the static EOM-UCC vectors, so the size-extensivity argument of Sec. S3 carries over.

Under $\hat{B} \to \hat{B} + c$ the right-hand side is invariant, whereas $\langle\Phi_I|\tilde{B}_T|\Phi_J\rangle \to \langle\Phi_I|\tilde{B}_T|\Phi_J\rangle + c\,S_{IJ}$. A transition moment between non-orthogonal states carries a disconnected piece $\langle\tilde{B}_T\rangle S_{IJ}$, which scales with system size because $\langle\tilde{B}_T\rangle$ does. Eq. (S29) isolates the linked remainder. It is possible to assume that $S_{IJ} = \delta_{IJ}$ since this will hold true in the FCI limit, the subtraction vanishes for $I \neq J$, and the right-hand side is the transition matrix element itself,

$$\langle\Phi_I|\tilde{B}_T|\Phi_J\rangle = \frac{1}{2}F_{\mathrm{C}}[z_I,z_J] - \frac{\mathrm{i}}{2}F_{\mathrm{C}}[z_I,w_J]\ , \qquad I \neq J\ . \tag{S30}$$

Two special cases follow from Eq. (S29) with no further work.

We now analyze ground-to-excited state elements. The reference $|\Phi_0\rangle = |0\rangle$ is not generated by an EOM vector. In Eq. (S11) it enters through the amplitude c_0 rather. The corresponding elements are thus obtained from Eq. (S21) with a single commutator. Using $z_I|0\rangle = |\Phi_I\rangle$ and $\langle 0|z_I = -\langle\Phi_I|$,

$$\langle[\tilde{B}_T,z_I]\rangle = \langle 0|\tilde{B}_T|\Phi_I\rangle + \langle\Phi_I|\tilde{B}_T|0\rangle = 2\,\mathrm{Re}\,\langle\Phi_I|\tilde{B}_T|\Phi_0\rangle\ , \tag{S31}$$

while the conjugate w_I, for which both signs are positive, gives

$$\langle[\tilde{B}_T,w_I]\rangle = \mathrm{i}\Big(\langle 0|\tilde{B}_T|\Phi_I\rangle - \langle\Phi_I|\tilde{B}_T|0\rangle\Big) = 2\,\mathrm{Im}\,\langle\Phi_I|\tilde{B}_T|\Phi_0\rangle\ . \tag{S32}$$

Hence

$$\langle \Phi_I | \tilde{B}_T | \Phi_0 \rangle = \frac{1}{2} \langle [\tilde{B}_T, z_I] \rangle + \frac{\mathrm{i}}{2} \langle [\tilde{B}_T, w_I] \rangle \ . \tag{S33}$$

And we also identify:

$$c_0^* \langle \tilde{B}_T \tilde{z}(0) \rangle - c_0 \langle \tilde{z}(0) \tilde{B}_T \rangle = 2 \, \mathrm{Re} \left(c_0 \langle \Phi_I | \tilde{B}_T | \Phi_0 \rangle \right) \ , \tag{S34}$$

so that $c_0 = 1$ and $c_0 = \mathrm{i}$ again select the real and imaginary parts.

We set $J = I$ in Eq. (S29) and $S_{II} = 1$, and consider Eq. (S26),

$$F_{\mathrm{C}}[z_I, w_I] = - \left(\langle z_I \, \delta \tilde{B}_T \, w_I \rangle + \langle w_I \, \delta \tilde{B}_T \, z_I \rangle \right) = - \left(-\mathrm{i} + \mathrm{i} \right) \langle \Phi_I | \delta \tilde{B}_T | \Phi_I \rangle = 0 \ . \tag{S35}$$

In contrast, $F_{\mathrm{C}}[z_I, z_I] = \langle [[\tilde{B}_T, z_I], z_I] \rangle - \langle \{ \tilde{B}_T, z_I^2 \} \rangle_{\mathrm{C}}$ from Eq. (S25), so:

$$\langle \Phi_I | \tilde{B}_T | \Phi_I \rangle = \langle \tilde{B}_T \rangle + \frac{1}{2} \langle [[\tilde{B}_T, z_I], z_I] \rangle - \frac{1}{2} \langle \{ \tilde{B}_T, z_I^2 \} \rangle_{\mathrm{C}} \ . \tag{S36}$$

This is precisely Eq. (S16) evaluated at $c_0 = 0$, $\tilde{z}(0) = z_I$ and $D = \langle -z_I^2 \rangle = 1$, which closes the consistency of the two sections. The excited-state expectation value is the superposition observable of Sec. S3 with the reference amplitude switched off. The above can be used to estimate said element, which converges to the FCI limit.

S4.2 Supermolecular additivity

We start from Eq. (S11) at $t = 0$, where $\hat{y}(0) = \hat{T}$ and $\tilde{B}_y(0) = \tilde{B}_T$. Let A and B be non-interacting, $|0\rangle = |0_{\mathrm{A}}\rangle \otimes |0_{\mathrm{B}}\rangle$, and $\hat{T} = \hat{T}_{\mathrm{A}} + \hat{T}_{\mathrm{B}}$ with $[\hat{T}_{\mathrm{A}}, \hat{T}_{\mathrm{B}}] = 0$. For $\hat{B} = \hat{B}_{\mathrm{A}} + \hat{B}_{\mathrm{B}}$ the transformed operator splits,

$$\tilde{B}_T = \tilde{B}_{\mathrm{A}} + \tilde{B}_{\mathrm{B}} \ , \qquad \tilde{B}_{\mathrm{X}} = e^{-\hat{T}_{\mathrm{X}}} \hat{B}_{\mathrm{X}} e^{\hat{T}_{\mathrm{X}}} \ , \qquad \mathrm{X} = \mathrm{A}, \ \mathrm{B} \ , \tag{S37}$$

because $\hat{T}_{\mathrm{B}}$ commutes with $\hat{B}_{\mathrm{A}}$ and conversely. The same split holds for $\tilde{B}_y(t)$ at later times as long as the Hamiltonian, the drive and the excitation space are local, so that $\hat{y}(t)$ stays additive.

Let z_{X} be anti-Hermitian and local to X, with $[z_{\mathrm{A}}, z_{\mathrm{B}}] = 0$, and write

$$|\phi_{\mathrm{X}}\rangle = z_{\mathrm{X}} |0_{\mathrm{X}}\rangle \ , \quad n_{\mathrm{X}} = \langle \phi_{\mathrm{X}} | \phi_{\mathrm{X}} \rangle = \langle -z_{\mathrm{X}}^2 \rangle \ , \quad b_{\mathrm{X}} = \langle 0_{\mathrm{X}} | \tilde{B}_{\mathrm{X}} | 0_{\mathrm{X}} \rangle \ , \quad t_{\mathrm{X}} = \langle 0_{\mathrm{X}} | \tilde{B}_{\mathrm{X}} | \phi_{\mathrm{X}} \rangle \ , \tag{S38}$$

with $b_{\mathrm{X}}^{\mathrm{exc}} = \langle \phi_{\mathrm{X}} | \tilde{B}_{\mathrm{X}} | \phi_{\mathrm{X}} \rangle / n_{\mathrm{X}}$; only the product $n_{\mathrm{X}} b_{\mathrm{X}}^{\mathrm{exc}}$ appears, so $n_{\mathrm{X}} \to 0$ is benign. Expectation values of operators on disjoint subsystems factorize. We also have that $\langle z_{\mathrm{X}} \rangle = \langle 0_{\mathrm{X}} | \phi_{\mathrm{X}} \rangle = 0$ from the convention $\tilde{X}^I \leftarrow \tilde{X}^I - \langle \tilde{X}^I \rangle \hat{1}$ of the main text; its role is examined at the end.

Let us consider the case of one subsystem being excited. We take $\tilde{z}(0) = z_{\mathrm{A}} + z_{\mathrm{B}}$, for which

$$[c_0 + \tilde{z}(0)] |0\rangle = c_0 |0\rangle + |\Phi_{\mathrm{A}}\rangle + |\Phi_{\mathrm{B}}\rangle \ , \qquad |\Phi_{\mathrm{X}}\rangle = z_{\mathrm{X}} |0\rangle \ , \tag{S39}$$

and three orthogonal components: $\langle 0 | \Phi_{\mathrm{X}} \rangle = \langle z_{\mathrm{X}} \rangle = 0$ and $\langle \Phi_{\mathrm{A}} | \Phi_{\mathrm{B}} \rangle = - \langle z_{\mathrm{A}} \rangle \langle z_{\mathrm{B}} \rangle = 0$. The generators commute, so $\langle -\tilde{z}^2(0) \rangle = n_{\mathrm{A}} + n_{\mathrm{B}} - 2 \langle z_{\mathrm{A}} \rangle \langle z_{\mathrm{B}} \rangle$, and the denominator is additive,

$$D = |c_0|^2 + n_{\mathrm{A}} + n_{\mathrm{B}} \ . \tag{S40}$$

Each matrix element reduces to local scalars. These are $\langle 0 | \tilde{B}_T | \Phi_{\mathrm{A}} \rangle = t_{\mathrm{A}}$, the $\tilde{B}_{\mathrm{B}}$ part eliminating because $\langle 0_{\mathrm{A}} | \phi_{\mathrm{A}} \rangle = 0$; $\langle \Phi_{\mathrm{A}} | \tilde{B}_T | \Phi_{\mathrm{A}} \rangle = n_{\mathrm{A}} (b_{\mathrm{A}}^{\mathrm{exc}} + b_{\mathrm{B}})$, the spectator contributing its ground value; and $\langle \Phi_{\mathrm{A}} | \tilde{B}_T | \Phi_{\mathrm{B}} \rangle = 0$. Collecting terms,

$$\langle \hat{B} \rangle_{\mathrm{AB}} = \frac{1}{D} \sum_{\mathrm{X}=\mathrm{A},\mathrm{B}} \Big[\left(|c_0|^2 + n_{\mathrm{Y}} \right) b_{\mathrm{X}} + n_{\mathrm{X}} b_{\mathrm{X}}^{\mathrm{exc}} + 2 \, \mathrm{Re} \left(c_0^* t_{\mathrm{X}} \right) \Big] \ . \qquad \mathrm{Y} \neq \mathrm{X} \ , \tag{S41}$$

X contributes its ground value with weight $(|c_0|^2 + n_\mathrm{Y})/D$, the probability that X is unexcited, its excited value with weight n_X/D, and a coherence term.

Note that $(|c_0|^2 + n_\mathrm{Y})/D + n_\mathrm{X}/D = 1$, and Eq. (S41) is of the form $\mathrm{Tr}(\hat{\rho}_\mathrm{A}\hat{B}_\mathrm{A}) + \mathrm{Tr}(\hat{\rho}_\mathrm{B}\hat{B}_\mathrm{B})$ over the reduced states of $|\bar{\Psi}(0)\rangle$. Each subsystem sees a normalized local distribution over its ground and excited values, with the other subsystem traced out. This is the desired physical expression.

For example, setting $z_\mathrm{B} = 0$ gives:

$$\langle \hat{B} \rangle_\mathrm{AB} = \frac{|c_0|^2 b_\mathrm{A} + n_\mathrm{A} b_\mathrm{A}^\mathrm{exc} + 2\,\mathrm{Re}\,(c_0^* t_\mathrm{A})}{|c_0|^2 + n_\mathrm{A}} + b_\mathrm{B} = \langle \hat{B}_\mathrm{A} \rangle_\mathrm{A}^\mathrm{exc} + \langle \hat{B}_\mathrm{B} \rangle_\mathrm{B}^\mathrm{gs} \;, \tag{S42}$$

the isolated A result plus the ground-state value of B.

Now consider simultaneous subsystem excitation. The doubly excited component needs a generator built from $z_\mathrm{A} z_\mathrm{B}$, which is Hermitian, so the admissible object is

$$\zeta = \mathrm{i}\, z_\mathrm{A} z_\mathrm{B} \;, \qquad \zeta^\dagger = -\zeta \;, \tag{S43}$$

of the imaginary-symmetric type $\hat{\kappa}_{\mu+N_\omega}$ of Eq. (S52), not the real antisymmetric $\hat{\kappa}_\mu$. Take $\tilde{z}(0) = \zeta$. Then $\langle \zeta \rangle = \mathrm{i}\langle z_\mathrm{A} z_\mathrm{B} \rangle = \mathrm{i}\langle z_\mathrm{A} \rangle \langle z_\mathrm{B} \rangle = 0$, which uses the separation as well as the convention. The weight is multiplicative,

$$\langle -\zeta^2 \rangle = \langle z_\mathrm{A}^2 z_\mathrm{B}^2 \rangle = n_\mathrm{A} n_\mathrm{B} \;, \qquad D = |c_0|^2 + n_\mathrm{A} n_\mathrm{B} \;. \tag{S44}$$

The state has two components, $c_0|0\rangle + \mathrm{i}\,|\phi_\mathrm{A}\rangle \otimes |\phi_\mathrm{B}\rangle$. A sum of one-subsystem operators cannot change the excitation of both at once, so the interference vanishes,

$$\langle 0|\tilde{B}_T|\,\phi_\mathrm{A}\phi_\mathrm{B}\rangle = t_\mathrm{A}\langle 0_\mathrm{B}|\phi_\mathrm{B}\rangle + t_\mathrm{B}\langle 0_\mathrm{A}|\phi_\mathrm{A}\rangle = 0 \;, \tag{S45}$$

and the diagonal element is $n_\mathrm{A} n_\mathrm{B}(b_\mathrm{A}^\mathrm{exc} + b_\mathrm{B}^\mathrm{exc})$. Hence

$$\langle \hat{B} \rangle_\mathrm{AB} = \frac{|c_0|^2\,(b_\mathrm{A} + b_\mathrm{B}) + n_\mathrm{A} n_\mathrm{B}\,(b_\mathrm{A}^\mathrm{exc} + b_\mathrm{B}^\mathrm{exc})}{|c_0|^2 + n_\mathrm{A} n_\mathrm{B}} \;, \tag{S46}$$

is a two-configuration average. One joint weight $n_\mathrm{A} n_\mathrm{B}$ now multiplies both subsystems instead of one weight each, making $z_\mathrm{B} \to 0$ eliminates ζ and returns $b_\mathrm{A} + b_\mathrm{B}$, so A cannot be excited alone. The reduced states are again mixed, so this is not a sum of isolated subsystem results; only at $c_0 = 0$, where both subsystems are excited. Eq. (S46) reduce to $b_\mathrm{A}^\mathrm{exc} + b_\mathrm{B}^\mathrm{exc}$. For m subsystems the weight involves $\prod_i n_i$, exponential in m, against the additive $\sum_i n_i$ of Eq. (S40), simultaneous excitations require high order operations.

A general initial superposition uses all four components,

$$\tilde{z}(0) = \alpha_\mathrm{A} z_\mathrm{A} + \alpha_\mathrm{B} z_\mathrm{B} + \beta\zeta \;, \tag{S47}$$

with α_A, α_B, β real, the three generators being anti-Hermitian and independent. The cross terms vanish, $\langle z_\mathrm{A} z_\mathrm{B} \rangle = \langle z_\mathrm{A} \zeta \rangle = \langle z_\mathrm{B} \zeta \rangle = 0$, so $\langle \tilde{z}(0) \rangle = 0$ and

$$D = |c_0|^2 + \alpha_\mathrm{A}^2 n_\mathrm{A} + \alpha_\mathrm{B}^2 n_\mathrm{B} + \beta^2 n_\mathrm{A} n_\mathrm{B} \;. \tag{S48}$$

This state is entangled for generic amplitudes, where two excited subsystems are correlated. Entanglement is described here because for an additive $\hat{B}$ a normalized state gives $\mathrm{Tr}(\hat{\rho}_\mathrm{A}\hat{B}_\mathrm{A}) + \mathrm{Tr}(\hat{\rho}_\mathrm{B}\hat{B}_\mathrm{B})$ over its reduced states. This requires, however, that Eq. (S11) be an expectation value of a normalized state, where D has to be the squared norm. Eq. (S48) is so, due to the requirement $\langle \tilde{z}(0) \rangle = 0$.

Role of the reference-component convention: Each z_X is free up to an anti-Hermitian constant as the equations of motion involve only commutators. Shifting the factors first, as the convention prescribes, and forming the product afterwards gives

$$\mathrm{i}\,(z_A - \langle z_A\rangle)\,(z_B - \langle z_B\rangle) = \zeta - \mathrm{i}\langle z_B\rangle z_A - \mathrm{i}\langle z_A\rangle z_B + \mathrm{i}\langle z_A\rangle\langle z_B\rangle \;, \tag{S49}$$

whereas forming the product first and shifting it afterwards gives

$$\zeta - \langle\zeta\rangle\hat{1} = \zeta - \mathrm{i}\langle z_A z_B\rangle\hat{1} \;. \tag{S50}$$

These are different operators. They differ by the single-excitation generators $-\mathrm{i}\langle z_B\rangle z_A - \mathrm{i}\langle z_A\rangle z_B$. Shifting z_A and z_B satisfies the condition $\langle\hat{\zeta}\rangle = 0$, but shifting ζ separately, using un-shifted z_X, can be problematic.

The convention is a shift by an averaged element. A shift of a factor does not shift the product as needed. Whichever prescription is available depends on how the manifold is closed. If the algebra contains the doubly excited generator as a member, ζ is an eigenvector and Eq. (S50) applies to it directly; if ζ is only reachable as a product of two vectors, Eq. (S49) is the rule. For these reasons $\langle\tilde{z}(0)\rangle = 0$ is a condition on the generator, and for a product generator it has to be imposed on the individual operators for additivity.

The argument assumes z_A and z_B lie separately in the algebraic space. As noted in the main text, a closed $\mathfrak{su}(M)$ need not be local, and a truncation that mixes the subsystems will induce small nonlocality leaks.

S5 Truncated Excitation Spaces

The results reported in the main text employ the full excitation space of the six-site hard-core boson model, for which the cluster expansion terminates at excitation order 6 and the propagation is equivalent, in principle, to FCI. To assess how the formalism behaves when the excitation space is truncated, we repeat the driven-dynamics simulations for dynamical excitations up to order 2, 3, 4, and 6, keeping the Hamiltonian, the initial linear combination, and the pulse parameters unchanged. In each case the TDUCC result is compared against the exact propagation restricted to the same truncated space, so that the comparison isolates the error of the UCC method from the error incurred by discarding higher excitations. The excellent agreement between CI and UCC is due to the nature of the Hamiltonian involving excitation/de-excitation operators, and where $\hat{b}^\dagger|1\rangle = 0$. In more general settings noticeable differences between the two are expected.

Figures S1 and S2 show the time-dependent dipole and the excited-state population ($|C_1(t)|^2$), respectively. The results indicate that the truncation is faithful to the excitation space it is given. The errors are due to the truncation itself: the order-2 space is too small to reproduce either the dipole envelope or the post-pulse population plateaus, while orders 3 and 4 progressively approach the untruncated (order-6, FCI) result. These plots evidence the mid-to-strong character of the ring correlation.

S5.1 Active space and CAS-CI eigenvectors

The simulations are initiated from states obtained by diagonalizing the Hamiltonian in a complete active space built from the no-boson and the six singly-occupied configurations of the ring. Writing each configuration as the occupation string

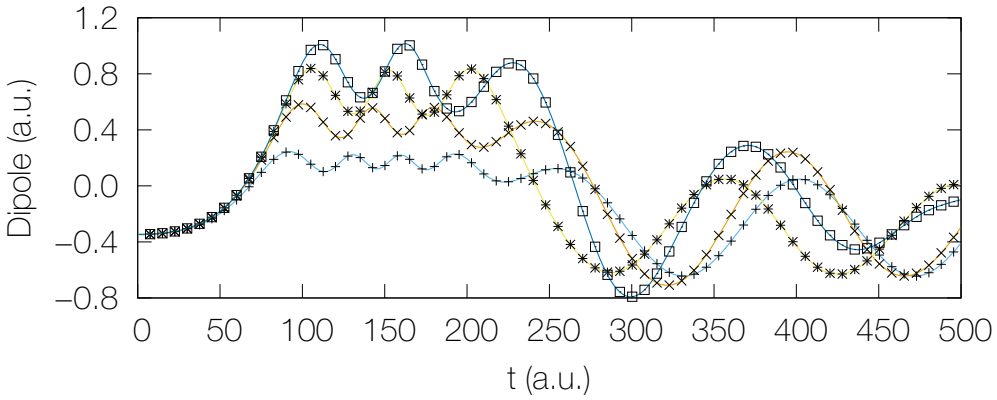

Figure S1. Time-dependent dipole of the six-site hard-core boson model computed with the excitation space truncated at order 2 (sky blue line, "+" symbols), 3 (orange line, "×" symbols), 4 (yellow line, "∗" symbols), and 6 (blue line, open-square symbols). Lines are the TDUCC results and points/symbols are the matching CI propagation within the same truncated space; order 6 spans the complete excitation manifold, so its reference is FCI.

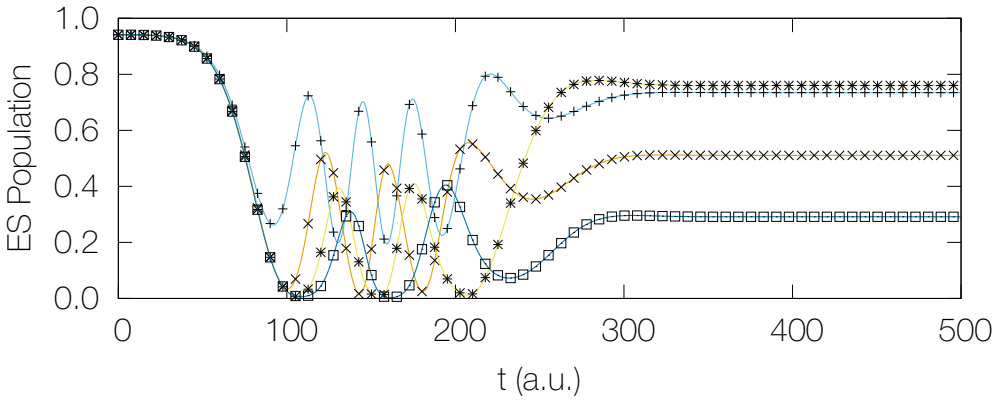

Figure S2. Excited-state populations for the same excitation-order scan as Fig. S1: truncation at order 2 (sky blue line, "+" symbols), 3 (orange line, "×" symbols), 4 (yellow line, "∗" symbols), and 6 (blue line, open square symbols), with TDUCC shown as lines and points/symbosl are the matching CI propagation, as in the previous figure.

$|n_1 n_2 n_3 n_4 n_5 n_6\rangle$ of the hard-core bosons, the active space is spanned, in the order used hereafter, by

$$\{\,\texttt{000000},\ \texttt{100000},\ \texttt{010000},\ \texttt{001000},\ \texttt{000100},\ \texttt{000010},\ \texttt{000001}\,\}\,, \tag{S51}$$

that is, the reference $|\Phi_0\rangle = |\texttt{000000}\rangle$ followed by the six configurations carrying a single excitation on site $p = 1, \ldots, 6$.

The resulting CAS-CI eigenvectors are displayed in Table S1, one row per eigenvector, with the columns ordered as in Eq. (S51). Only two eigenvectors, $K = 1$ and $K = 7$, carry any amplitude on the no-boson reference: they are a 2×2 rotation. The remaining five eigenvectors, $K = 2, \ldots, 6$, have strictly zero no-boson reference amplitude and span the orthogonal complement of $|S\rangle$ inside the single-excitation space. Their coefficient patterns are the combinations of the six-site ring. $K = 2$ alternates in sign from site to site, while $(K = 3, 4)$ and $(K = 5, 6)$ form pairs with three-site and six-site periodicity, respectively. Because each pair is degenerate, the particular linear combination returned within a pair is arbitrary; only the two-dimensional subspace it spans is determined.

Table S1. CAS-CI eigenvectors of the six-site hard-core boson model, given as row vectors in the active-space basis of Eq. (S51). Coefficients are rounded to four decimals; entries reported by the diagonalization at 10^{-15} magnitude or below are reported as 0. Each row is normalized to unity.

	Active-space configuration						
K	000000	100000	010000	001000	000100	000010	000001
1	−0.9345	0.1453	0.1453	0.1453	0.1453	0.1453	0.1453
2	0	0.4082	−0.4082	0.4082	−0.4082	0.4082	−0.4082
3	0	−0.5774	0.2887	0.2887	−0.5774	0.2887	0.2887
4	0	0	0.5000	−0.5000	0	0.5000	−0.5000
5	0	0.5774	0.2887	−0.2887	−0.5774	−0.2887	0.2887
6	0	0	0.5000	0.5000	0	−0.5000	−0.5000
7	0.3559	0.3815	0.3815	0.3815	0.3815	0.3815	0.3815

S5.2 Ground-state and excitation energies

We now compare the UCC and CI eigenvalue spectra order by order. Truncating the excitation manifold at order m involves $\sum_{k=0}^{m} \binom{6}{k}$ configurations, so the four orders appearing in Figs. S1 and S2 support 64, 57, 42 and 22 states, and hence 63, 56, 41 and 21 excitation energies, at orders 6, 4, 3 and 2 respectively. Ground-state energies for all four orders are shown in Table S2; the excitation energies $\omega_n = E_n - E_0$ are given in Tables S3, S4, S5 and S6. The two error scales are summarized across orders in Table S7. All energies are in atomic units; the eigenvalues are real to within the imaginary residue of the diagonalization, which is discarded.

We consider order 6 case. Here the unitary CC method should be "numerically exact". This is the reference point against which the truncated spaces are read. The agreement is indeed at the level of double-precision arithmetic, as expected. The ground-state energies differ by 5×10^{-18} a.u. For the excitation energies, each entry of the UCC and FCI columns of Table S3 agree in the twelve printed decimals. The residuals listed in the Δ_n columns are below 3×10^{-14} a.u., show a mean absolute deviation of 2×10^{-14} a.u. and a maximum relative deviation of 2×10^{-13}. The residuals grow slowly with ω_n, consistent with a deviation that scales with the magnitude of the root, and are uniformly negative. We also note the degeneracy pattern of the ring. This is already visible in the CAS-CI vectors of Table S1. Forty of the sixty-three roots group into twenty degenerate pairs ($n = 2, 3$; $4, 5$; $8, 9$; $10, 11$; and so on), with splittings of at most 4×10^{-15} a.u. (numerically exact degeneracies).

Table S2. Ground-state energy of the six-member hard-core boson model as a function of the excitation order, computed by CI and by the unitary coupled-cluster theory, in atomic units. At order 6 the CI result is FCI. The residual $\Delta_0 = E_0^{\mathrm{UCC}} - E_0^{\mathrm{CI}}$ measures the error of the unitary theory within a given space; the last column is the truncation error relative to FCI.

Order	E_0^{CI}	E_0^{UCC}	Δ_0	$E_0^{\mathrm{CI}} - E_0^{\mathrm{FCI}}$
6	−0.007702889420812862	−0.007702889420812867	-5.2×10^{-18}	0
4	−0.007691355150483798	−0.007691355150483777	$+2.1 \times 10^{-17}$	1.153×10^{-5}
3	−0.007665909340320160	−0.007665909340320138	$+2.3 \times 10^{-17}$	3.698×10^{-5}
2	−0.007629486442738102	−0.007629486442738093	$+8.7 \times 10^{-18}$	7.340×10^{-5}

Table S3. Complete set of 63 excitation energies $\omega_n = E_n - E_0$ of the six-site hard-core boson model at excitation order 6, from FCI and from the unitary coupled-cluster theory, in atomic units and rounded to twelve decimals. The residual $\Delta_n = \omega_n^{\mathrm{UCC}} - \omega_n^{\mathrm{FCI}}$ is given in units of 10^{-15} a.u. (so an entry of −15.6 means -1.56×10^{-14} a.u.). The single visible discrepancy in the printed digits, at $n = 12$, is a rounding artifact of the twelfth decimal. Imaginary parts of the UCC eigenvalues, of order 10^{-17} or smaller, are discarded.

n	ω_n^{FCI}	ω_n^{UCC}	Δ_n	n	ω_n^{FCI}	ω_n^{UCC}	Δ_n
1	0.035639072276	0.035639072276	−5.0	33	0.138957290952	0.138957290952	−18.3
2	0.037803639359	0.037803639359	−6.9	34	0.141044348669	0.141044348669	−18.3
3	0.037803639359	0.037803639359	−5.1	35	0.141547264915	0.141547264915	−19.2
4	0.042102785851	0.042102785851	−8.8	36	0.154589469637	0.154589469637	−15.8
5	0.042102785851	0.042102785851	−6.0	37	0.154617667861	0.154617667861	−15.7
6	0.044236244873	0.044236244873	−8.4	38	0.154617667861	0.154617667861	−15.2
7	0.073382772583	0.073382772583	−11.7	39	0.154726633758	0.154726633758	−16.3
8	0.076694469038	0.076694469038	−13.1	40	0.154726633758	0.154726633758	−15.7
9	0.076694469038	0.076694469038	−12.0	41	0.154839897523	0.154839897523	−15.6
10	0.079088088628	0.079088088628	−14.2	42	0.187733022369	0.187733022369	−19.2
11	0.079088088628	0.079088088628	−11.6	43	0.190870316913	0.190870316913	−21.2
12	0.079764732248	0.079764732247	−13.2	44	0.190870316913	0.190870316913	−20.9
13	0.082759487089	0.082759487089	−14.5	45	0.193208867783	0.193208867783	−22.8
14	0.082759487089	0.082759487089	−13.4	46	0.193208867783	0.193208867783	−19.9
15	0.085271809083	0.085271809083	−14.7	47	0.193910536658	0.193910536658	−20.8
16	0.097012748507	0.097012748507	−10.4	48	0.196578112059	0.196578112059	−22.6
17	0.097255876154	0.097255876154	−11.7	49	0.196578112059	0.196578112059	−22.1
18	0.097255876154	0.097255876154	−10.3	50	0.198941190711	0.198941190711	−20.9
19	0.097722452665	0.097722452665	−11.9	51	0.211377571086	0.211377571086	−19.9
20	0.097722452665	0.097722452665	−10.5	52	0.211623556296	0.211623556296	−20.9
21	0.098072969035	0.098072969035	−11.9	53	0.211623556296	0.211623556296	−18.7
22	0.117780046037	0.117780046037	−18.0	54	0.212085095499	0.212085095499	−21.1
23	0.118383840712	0.118383840712	−19.0	55	0.212085095499	0.212085095499	−18.3
24	0.132656889421	0.132656889421	−16.6	56	0.212407504732	0.212407504732	−18.1
25	0.134012605772	0.134012605772	−17.2	57	0.264365763319	0.264365763319	−23.9
26	0.134324721899	0.134324721899	−16.6	58	0.266400646009	0.266400646009	−24.6
27	0.134324721899	0.134324721899	−16.2	59	0.266400646009	0.266400646009	−22.8
28	0.134758151421	0.134758151421	−17.1	60	0.270464290902	0.270464290902	−23.6
29	0.134758151421	0.134758151421	−16.9	61	0.270464290902	0.270464290902	−23.3
30	0.138415638280	0.138415638280	−17.6	62	0.272493593954	0.272493593954	−20.8
31	0.138415638280	0.138415638280	−17.7	63	0.343085451979	0.343085451979	−27.0
32	0.138957290952	0.138957290952	−18.5				

For order 4, truncating at quadruple excitations removes seven of the sixty-four configurations, resulting in 57 states and 56 excitation energies. The the UCC–CI residual is unchanged by the truncation. The ground-state energies of Table S2 differ by 2×10^{-17} a.u., and the excitation-energy residuals of Table S4 are below 2×10^{-14} a.u., showing a mean absolute deviation of 10^{-14} a.u. These are the same magnitudes found at order 6. The unitary method reproduces the CI spectrum down to the numerical "floor" of the calculation. Truncating the space does not degrade it. As expected, the truncation changes the spectrum itself. The order-4 ground state lies 1.2×10^{-5} a.u. above FCI. The excitation energies deviate from their FCI counterparts by up to 1.5×10^{-3} a.u. (0.9% in relative terms), giving a mean absolute deviation of 2×10^{-4} a.u. over its 56 roots. It can be inferred that the spread between curves of different order is truncation. We note that the comparison to FCI matches roots by ascending order, and that the two orderings are not entirely in correspondence. The 57-state spectrum has a degenerate pair at $n = 25, 26$ where the full spectrum has a pair at $n = 26, 27$, so individual assignments near that crossing should be read with care.

Table S4. The 56 excitation energies for order 4; same as before, from CI and from the unitary coupled-cluster theory, in atomic units, rounded to twelve decimals. Every pair of CI and UCC entries agrees in all twelve printed decimals. Imaginary parts of the UCC eigenvalues, of order 10^{-17} or smaller, are discarded.

n	ω_n^{CI}	ω_n^{UCC}	Δ_n	n	ω_n^{CI}	ω_n^{UCC}	Δ_n
1	0.035630978317	0.035630978317	−9.1	29	0.134748265907	0.134748265907	−11.8
2	0.037796106615	0.037796106615	−10.0	30	0.138526425911	0.138526425911	−13.4
3	0.037796106615	0.037796106615	−9.8	31	0.138526425911	0.138526425911	−12.8
4	0.042097047198	0.042097047198	−12.1	32	0.139434826257	0.139434826257	−12.1
5	0.042097047198	0.042097047198	−10.3	33	0.139434826257	0.139434826257	−11.4
6	0.044346532931	0.044346532931	−7.0	34	0.141032814399	0.141032814399	−13.4
7	0.073375695385	0.073375695385	−11.1	35	0.142830527643	0.142830527643	−15.3
8	0.076683543959	0.076683543959	−12.4	36	0.154590197620	0.154590197620	−10.8
9	0.076683543959	0.076683543959	−12.0	37	0.154608254018	0.154608254018	−11.3
10	0.079087986878	0.079087986878	−13.1	38	0.154608254018	0.154608254018	−10.5
11	0.079087986878	0.079087986878	−12.4	39	0.155049313761	0.155049313761	−11.0
12	0.079798179605	0.079798179605	−11.5	40	0.155049313761	0.155049313761	−11.0
13	0.082799743038	0.082799743038	−12.9	41	0.155949151467	0.155949151467	−13.8
14	0.082799743038	0.082799743038	−13.0	42	0.187756341351	0.187756341351	−12.1
15	0.085518509004	0.085518509004	−13.1	43	0.190872073956	0.190872073956	−12.4
16	0.097001214237	0.097001214237	−11.1	44	0.190872073956	0.190872073956	−12.5
17	0.097247413055	0.097247413055	−11.3	45	0.193368838378	0.193368838378	−12.4
18	0.097247413055	0.097247413055	−10.2	46	0.193368838378	0.193368838378	−10.6
19	0.097755416307	0.097755416307	−10.3	47	0.194868197755	0.194868197755	−5.0
20	0.097755416307	0.097755416307	−10.2	48	0.197328164116	0.197328164116	−8.6
21	0.098366465503	0.098366465503	−9.5	49	0.197328164116	0.197328164116	−7.8
22	0.117946949558	0.117946949558	−14.5	50	0.200411258396	0.200411258396	−12.6
23	0.118482871746	0.118482871746	−14.0	51	0.211366036816	0.211366036816	−11.0
24	0.132645355150	0.132645355150	−11.5	52	0.211638813651	0.211638813651	−11.8
25	0.134314048756	0.134314048756	−12.3	53	0.211638813651	0.211638813651	−9.3
26	0.134314048756	0.134314048756	−11.5	54	0.212347552103	0.212347552103	−7.1
27	0.134336779305	0.134336779305	−10.5	55	0.212347552103	0.212347552103	−5.7
28	0.134748265907	0.134748265907	−12.6	56	0.213769170474	0.213769170474	−6.8

For order 3, truncating at triple excitations leaves 42 states and 41 excitation energies. The trends established at order 4 are confirmed without change. The UCC and CI ground-state energies differ by 2×10^{-17} a.u., and the excitation-energy residuals of Table S5 stay below 2×10^{-14} a.u., with a mean absolute deviation of 10^{-14} a.u., indistinguishable from the orders 4 and 6 figures. Across the three orders the method error is flat, at roughly 10^{-14} a.u., and shows no dependence on the size of the space.

The truncation error, by contrast, grows monotonically as excitations are removed. The order-3 ground state lies 3.7×10^{-5} a.u. above FCI, three times the

order-4 value, and the excitation energies depart from their FCI counterparts by up to 1.6×10^{-3} a.u. (1.3%), with a mean absolute deviation of 3×10^{-4} a.u. over its 41 roots. A comparison against order 4 is shown in Table S7, since the two spaces support different numbers of roots and the deviations grow with ω_n. The ordering caveat noted for order 4 applies here as well. The order-3 spectrum has a degenerate pair at $n = 25, 26$ where the full spectrum has one at $n = 26, 27$.

Table S5. The 41 excitation energies for order 3 truncation.

n	ω_n^{CI}	ω_n^{UCC}	Δ_n	n	ω_n^{CI}	ω_n^{UCC}	Δ_n
1	0.035620724740	0.035620724740	−10.8	22	0.118281264884	0.118281264884	−15.2
2	0.037789921752	0.037789921752	−11.6	23	0.118941842989	0.118941842989	−12.8
3	0.037789921752	0.037789921752	−11.6	24	0.132619909340	0.132619909340	−14.9
4	0.042103425218	0.042103425218	−13.1	25	0.134425608834	0.134425608834	−11.1
5	0.042103425218	0.042103425218	−13.0	26	0.134425608834	0.134425608834	−11.1
6	0.044505628368	0.044505628368	−18.0	27	0.134527095886	0.134527095886	−7.8
7	0.073400227952	0.073400227952	−13.3	28	0.134880339164	0.134880339164	−11.4
8	0.076732033757	0.076732033757	−14.6	29	0.134880339164	0.134880339164	−11.4
9	0.076732033757	0.076732033757	−14.6	30	0.138724196926	0.138724196926	−14.5
10	0.079200708352	0.079200708352	−14.8	31	0.138724196926	0.138724196926	−14.5
11	0.079200708352	0.079200708352	−14.8	32	0.139790130672	0.139790130672	−6.4
12	0.080176223708	0.080176223708	−13.4	33	0.139790130672	0.139790130672	−6.5
13	0.083216450819	0.083216450819	−15.2	34	0.141410910021	0.141410910021	−12.0
14	0.083216450819	0.083216450819	−15.1	35	0.143132023529	0.143132023529	−9.6
15	0.086122860373	0.086122860373	−15.6	36	0.154605921911	0.154605921911	−13.7
16	0.097004276944	0.097004276944	−12.6	37	0.154667730712	0.154667730712	−11.0
17	0.097322335876	0.097322335876	−12.7	38	0.154667730712	0.154667730712	−10.9
18	0.097322335876	0.097322335876	−12.8	39	0.155216518009	0.155216518009	−7.0
19	0.098154908432	0.098154908432	−12.2	40	0.155216518009	0.155216518009	−6.3
20	0.098154908432	0.098154908432	−12.2	41	0.156182776365	0.156182776365	−6.8
21	0.099386274545	0.099386274545	−11.5				

Let us consider order 2. The smallest space considered keeps only the reference, the six single and the fifteen double excitations, giving 22 states and 21 excitation energies. The UCC error again does not change. The ground-state energies differ by 9×10^{-18} a.u., and the residuals of Table S6 are below 1.5×10^{-14} a.u.; mean absolute deviation of 9×10^{-15} a.u. The truncation error, on the other hand, is now at its largest. The ground state is 7.3×10^{-5} a.u. above FCI, and the excitation energies are displaced by up to 1.5×10^{-3} a.u., which at these low-lying frequencies amounts to 2.8%. In contrast to the larger spaces, each order-2 excitation energy is above its FCI counterpart. The degeneracy pattern of the lowest 21 roots matches the full spectrum, so no ordering caveat is needed here.

Table S7 shows the two error scales across all four orders. The truncation error evaluated over the lowest 21 roots so that the four spaces are compared on a common set of states. It makes the central point of this section quantitative. The UCC error is flat at $\sim 10^{-14}$ a.u. over spaces ranging from 22 to 64 states. The truncation error, in contrast, rises by an order of magnitude from order 4 to order 2, from 0.3% to 2.8% in the worst case. The two scales are separated by ten orders of magnitude, which is why the curves of Figs. S1 and S2 may be read as a measure of excitation-space truncation.

The excitation basis results from decomposition of their metric $\tilde{S}_{kl} = \langle 0|\hat{\tau}_k^\dagger \hat{\tau}_l|0\rangle$, keeping those singular vectors whose singular values s exceed a threshold $\eta = 10^{-6}$ and rescaling them by $s^{-1/2}$. In all cases reported in this section, covering all four excitation orders, the singular values are between 0.3 and 1.9. They are not tabulated, as only this range is relevant here. We note now that: i) The smallest singular value is five orders of magnitude above η. No meaningful direction is discarded, and the excitation basis is of full rank within each truncation. From the

$\sum_{k=0}^{m}\binom{6}{k}$ states none is removed for linear dependence. ii) Their metric is well conditioned, with a ratio of largest to smallest singular value of at most 7. The $s^{-1/2}$ rescaling amplifies no component by more than $s_{\min}^{-1/2} \approx 2$. Neither figure degrades as the space is truncated, consistent with the uniform 10^{-14} a.u. residuals found at every order.

The dominant contribution of error is the convergence of the ground-state amplitudes. The iteration is stopped once the amplitude step falls below 10^{-13}, the residual error of the converged vector can be read directly from Table S8. The amplitudes forbidden by the symmetry of the reference, which should vanish identically, instead are at up to 4×10^{-13}. An amplitude error δt enters E_0 at around second order. This is why the ground-state columns of Table S2 agree to 10^{-17}–10^{-18} a.u. The excitation energies behave differently. The Jacobian depends on the amplitudes through $\hat{H}_T = e^{-\hat{T}}\hat{H}_0 e^{\hat{T}}$, whose first-order variation is $[\hat{H}_T, \delta\hat{T}]$, so the induced shift is linear in the amplitude error, $\delta\Omega \sim \|\hat{H}_0\|\,\delta t$. With the spectrum of $\hat{H}_0$ spanning $\sim 10^{-1}$ a.u., this places the floor in the low 10^{-14} a.u. range, as Table S7 reports.

It follows that the intrinsic error of the truncated UCC method is smaller than the values tabulated here, so the ten-order-of-magnitude separation from the truncation error can be understated. Resolving the true figure would require tightening the amplitude convergence threshold, which would not change conclusions drawn in this section. We note that the lowest excitation is non-degenerate at all four orders (ω_1 and ω_2 are separated by $\approx 2 \times 10^{-3}$ a.u., the first degenerate pair being $n = 2, 3$). The eigenvector of Sec. S5.4 and the initial state built from it in the time-dependent simulations are uniquely determined.

Table S6. 21 excitation energies for order 2 excitation truncation.

n	ω_n^{CI}	ω_n^{UCC}	Δ_n	n	ω_n^{CI}	ω_n^{UCC}	Δ_n
1	0.035782101919	0.035782101919	−9.0	12	0.080457387974	0.080457387974	−6.6
2	0.037965298549	0.037965298549	−9.7	13	0.083298300865	0.083298300865	−7.2
3	0.037965298549	0.037965298549	−9.7	14	0.083298300865	0.083298300865	−7.0
4	0.042329551518	0.042329551518	−11.2	15	0.086295321439	0.086295321439	−10.3
5	0.042329551518	0.042329551518	−11.1	16	0.097013638081	0.097013638081	−9.9
6	0.045495720897	0.045495720897	−13.8	17	0.097401317992	0.097401317992	−8.6
7	0.073451728134	0.073451728134	−9.9	18	0.097401317992	0.097401317992	−8.7
8	0.076797663930	0.076797663930	−9.8	19	0.098288060080	0.098288060080	−5.0
9	0.076797663930	0.076797663930	−9.8	20	0.098288060080	0.098288060080	−4.9
10	0.079295610403	0.079295610403	−9.7	21	0.099594878190	0.099594878190	−4.6
11	0.079295610403	0.079295610403	−9.7				

Table S7. The two error scales of the excitation-order scan, in atomic units. "States" is the dimension $\sum_{k=0}^{m}\binom{6}{k}$ of the truncated space and N_ω the number of excitation energies it supports. The method error $\Delta_n = \omega_n^{\mathrm{UCC}} - \omega_n^{\mathrm{CI}}$ is taken over all N_ω roots of the given order. The truncation error $\delta_n = \omega_n^{\mathrm{CI}} - \omega_n^{\mathrm{FCI}}$ is evaluated over the lowest 21 roots only, common to all four spaces, so that the orders are compared on the same set of states; the relative column is $\max_n |\delta_n/\omega_n^{\mathrm{FCI}}|$ over that set. Roots are matched by ascending order.

			Method error		Truncation error		
Order	States	N_ω	mean $\lvert\Delta_n\rvert$	max $\lvert\Delta_n\rvert$	mean $\lvert\delta_n\rvert$	max $\lvert\delta_n\rvert$	max rel.
6	64	63	1.7×10^{-14}	2.7×10^{-14}	0	0	0
4	57	56	1.1×10^{-14}	1.5×10^{-14}	4.4×10^{-5}	2.9×10^{-4}	0.30%
3	42	41	1.2×10^{-14}	1.8×10^{-14}	2.4×10^{-4}	1.3×10^{-3}	1.34%
2	22	21	8.9×10^{-15}	1.4×10^{-14}	4.1×10^{-4}	1.5×10^{-3}	2.85%

S5.3 Converged cluster amplitudes

It is instructive to look at the converged ground-state cluster operator itself. The generator basis is built in pairs from the orthonormalized excitation operators $\hat{\tau}_\mu$ of Sec. S5.2: for each $\mu = 1, \ldots, N_\omega$ one forms a real antisymmetric generator and an imaginary symmetric one,

$$\hat{\kappa}_\mu = \hat{\tau}_\mu - \hat{\tau}_\mu^\dagger \,, \qquad \hat{\kappa}_{\mu+N_\omega} = \mathrm{i}\left(\hat{\tau}_\mu + \hat{\tau}_\mu^\dagger\right) \,, \tag{S52}$$

so that $\hat{T} = \sum_{\mu=1}^{2N_\omega} t_\mu \hat{\kappa}_\mu$. The amplitude vector therefore has $2N_\omega$ entries: 126, 112, 82 and 42 at orders 6, 4, 3 and 2.

For ground state, the entire second block ($\mu + N_\omega$) vanishes identically, as exact zeros at every order. The static ground-state cluster operator uses only the real antisymmetric basis operators, $e^{\hat{T}}$ is then a real orthogonal rotation; no imaginary-symmetric component is needed. Within the non-vanishing block only about half the amplitudes are nonzero, 33 of 63 at order 6, 31 of 56 at order 4, 21 of 41 at order 3 and 11 of 21 at order 2. The remainder are numerically vanishing, bounded by 5×10^{-13}, regardless of order; these are amplitudes forbidden by the symmetry of the reference. The consistency of the fraction across four differently sized spaces suggests a symmetry selection rule. However, we did not the basis by irreducible representations in this work.

Table S8 lists the non-negligible amplitudes. The norm of the cluster vector is almost independent of the truncation, $\|\mathbf{t}\| \approx 0.109$ at all four orders, a spread of about one percent across spaces differing by a factor of three in size. How the fixed total is distributed changes, however: the largest single amplitude grows monotonically as the space contracts, from 0.069 at order 6 to 0.108 at order 2, where a single component carries almost the entire norm. The cluster operator does not shrink when excitations are removed, it concentrates instead. This is consistent with the ground-state energies of Table S2.

S5.4 First EOM-UCC excitation vector

The dynamics of Figs. S1 and S2 are initiated from a linear combination of the ground state and the lowest excited state, the latter generated by the first EOM-UCC eigenvector. Since that vector fixes the initial condition, we record it here. The frequency it belongs to is ≈ 0.036 a.u. at all four orders, given to full precision by the $n = 1$ UCC entries of Tables S3–S6.

The eigenvector is written $\tilde{X}^I = \sum_\nu X_\nu^I \hat{\Xi}_{0,\nu}$ with $\hat{\Xi}_{0,\nu} = \hat{\pi}_T(\hat{\kappa}_\nu)$, so its $2N_\omega$ components are labeled by the paired generator basis of Eq. (S52). The eigenvector effects the dynamics through the initial generator $\tilde{z}(0) = \sum_{I>0}(c_I \tilde{X}^I - c_I^* \tilde{X}^{I\dagger})$ of the main text. Since the $\hat{\Xi}_{0,\nu}$ are anti-Hermitian, $\tilde{X}^{I\dagger} = -\sum_\nu (X_\nu^I)^* \hat{\Xi}_{0,\nu}$, the combination antisymmetrizes to

$$\tilde{z}(0) = \sum_{I>0} \sum_\nu 2\,\mathrm{Re}\left(c_I X_\nu^I\right) \hat{\Xi}_{0,\nu} \,. \tag{S53}$$

Only $\mathrm{Re}(c_I X_\nu^I)$ remains. Additionally, an eigenvector of the generalized problem is fixed up to a global complex factor, which can be absorbed into c_I. The state depends on the product $c_I \tilde{X}^I$, not on the two separately.

We fix the phase by requiring the largest component on the real antisymmetric block to be real, the residual sign by requiring positive overlap with the corresponding CI excited state, which makes the anchoring entry ($\mu = 26$, 37, 19 and 1 at orders 6, 4, 3 and 2) negative at orders 3 and 2. Under this convention the

Table S8. Converged ground-state cluster amplitudes t_μ of $\hat{T} = \sum_\mu t_\mu \hat{\kappa}_\mu$, for each excitation order. Only the amplitudes of the real antisymmetric generators $\hat{\kappa}_\mu = \hat{\tau}_\mu - \hat{\tau}_\mu^\dagger$ are shown, and from those only the terms exceeding 10^{-10} in magnitude. The amplitudes omitted from this block are numerically zero (below 4.2×10^{-13} at any order), and the amplitudes of the imaginary-symmetric generators $\mathrm{i}(\hat{\tau}_\mu + \hat{\tau}_\mu^\dagger)$ are zero and are not listed. The index μ labels each order's own SVD- and QR-adapted generator basis and is not comparable between columns: the four spaces have different dimensions and their bases are constructed independently.

Order 6		Order 4		Order 3		Order 2	
μ	t_μ	μ	t_μ	μ	t_μ	m	t_μ
1	0.06879744	6	0.06420044	6	−0.08886644	6	−0.10816584
7	0.02983811	7	−0.00007443	7	0.00026546	7	0.00033215
13	−0.00108730	8	0.00179527	8	−0.00056626	8	−0.00039818
14	−0.00091403	9	0.00213987	9	0.00321174	9	−0.00114467
15	0.00070310	10	−0.00105710	10	−0.00212255	10	0.00361245
16	−0.00108404	11	−0.00229692	11	0.00211404	11	−0.00075070
17	0.00005609	12	−0.00196333	12	−0.00270004	12	0.00189317
18	0.00181999	13	−0.00248476	13	0.00182995	13	−0.00053871
19	0.00123370	14	0.00021818	14	0.00308483	14	−0.00682671
20	0.00081749	15	−0.00012737	15	−0.00146654	15	0.00121313
21	−0.00389021	21	−0.07996618	26	−0.06020010	21	0.01240209
22	−0.06901746	22	−0.00075836	27	0.00054988		
28	0.00225817	23	−0.00484906	28	0.00014475		
29	−0.00235665	24	−0.00033903	29	−0.00071229		
30	0.00068059	25	−0.00022298	30	0.00199964		
31	0.00003163	26	0.00116132	31	0.00197928		
32	−0.00007583	27	0.00268338	32	0.00102276		
33	0.00131390	28	−0.00060300	33	0.00201415		
34	−0.00030189	29	−0.00131597	34	0.00348872		
35	−0.00190139	30	−0.00118040	35	0.00083230		
36	−0.00443156	41	−0.00833795	41	0.01327970		
42	0.01128379	42	0.00071382				
48	−0.00013957	43	−0.00060894				
49	0.00110990	44	0.00101409				
50	0.00142199	45	0.00017157				
51	−0.00249389	46	−0.00087724				
52	−0.00052648	47	−0.00211920				
53	−0.00009684	48	0.00018061				
54	0.00008557	49	0.00036935				
55	−0.00150723	50	0.00186543				
56	−0.00006557	56	0.03603878				
57	0.02150804						
63	0.03157080						

first block, real antisymmetric generators $\hat{\kappa}_\mu$, is purely real and the second block, imaginary-symmetric $\hat{\kappa}_{\mu+N_\omega}$, purely imaginary, both to 1.4×10^{-15} or better in general. With real c_I the second block drops out of Eq. (S53). The first column of each panel of Table S9 is the vector that builds the initial condition.

As with the cluster amplitudes of Sec. S5.3, roughly half of the components vanish, 30 of 63, 25 of 56, 20 of 41 and 10 of 21 surviving, the same index set is nonzero in both blocks. The block norms are insensitive to the truncation, ≈ 0.497 for the first and ≈ 0.507 for the second at all four orders. The same behavior is already seen in Table S8.

Table S9. First EOM-UCC excitation vector at each excitation order, in the generator basis of Eq. (S52). For each order, $\mathrm{Re}\, X_\mu$ is the coefficient of the real antisymmetric generator $\hat{\kappa}_\mu = \hat{\tau}_\mu - \hat{\tau}_\mu^\dagger$ and $\mathrm{Im}\, X_{\mu'}$, with $\mu' = \mu + N_\omega$, that of the paired imaginary-symmetric generator $\mathrm{i}(\hat{\tau}_\mu + \hat{\tau}_\mu^\dagger)$. Only $2\,\mathrm{Re}(c_I X_\nu)$ enters the initial generator, Eq. (S53); with the phase convention used here and real c_I that is the first block alone, and the second is listed only to show that the convention is met. The first block is real and the second purely imaginary to 1.4×10^{-15} or better, so the two omitted parts of each entry are "numerical" zeros. Only components exceeding 10^{-10} are shown; the same index set is nonzero in both blocks. The phase is fixed so that the largest first-block component is real, and the residual sign so that the state overlaps the corresponding CI state positively. The index μ labels each order's own generator basis and is not comparable between columns.

Order 6			Order 4			Order 3			Order 2		
μ	$\mathrm{Re}\, X_\mu$	$\mathrm{Im}\, X_{\mu'}$	μ	$\mathrm{Re}\, X_\mu$	$\mathrm{Im}\, X_{\mu'}$	μ	$\mathrm{Re}\, X_\mu$	$\mathrm{Im}\, X_{\mu'}$	μ	$\mathrm{Re}\, X_\mu$	$\mathrm{Im}\, X_{\mu'}$
2	0.07277689	−0.07417270	1	−0.00984646	0.01007296	1	0.05793987	−0.05870815	1	−0.29387447	0.30200544
3	−0.07897602	0.08049072	2	0.07815983	−0.07995774	2	−0.15877790	0.16088329	2	−0.02773292	0.02850024
4	−0.04624741	0.04713440	3	−0.13034091	0.13333915	3	0.14643150	−0.14837318	3	−0.16318744	0.16770254
5	0.08492923	−0.08655810	4	−0.05125001	0.05242892	4	−0.03224959	0.03267722	4	0.10904473	−0.11206179
6	−0.06994981	0.07129139	5	−0.08364807	0.08557223	5	0.11687713	−0.11842691	5	−0.14488246	0.14889109
8	−0.03136786	0.03200192	16	−0.11477365	0.11679319	16	−0.20867423	0.21414017	16	−0.05360857	0.05423198
9	0.15217221	−0.15524816	17	0.18205084	−0.18525418	17	−0.00988757	0.01014656	17	−0.17171007	0.17370685
10	−0.10210256	0.10416642	18	0.17804043	−0.18117320	18	0.09804108	−0.10060913	18	−0.11839243	0.11976919
11	0.21249670	−0.21679203	19	0.19147812	−0.19484734	19	−0.30719355	0.31524007	19	−0.11449537	0.11582682
12	−0.04268645	0.04354930	20	0.00420027	−0.00427418	20	−0.02400756	0.02463640	20	0.20257042	−0.20492608
23	0.06137529	−0.06268538	31	0.00053351	−0.00056999	21	−0.00011411	0.00011442			
24	0.07147988	−0.07300567	32	−0.00022778	0.00022659	22	0.00017395	−0.00017640			
25	−0.04455307	0.04550408	33	0.00008556	−0.00010182	23	0.00021068	−0.00021764			
26	0.25381339	−0.25923121	34	−0.00037026	0.00038923	24	0.00070650	−0.00072573			
27	−0.12731785	0.13003553	35	0.00021728	−0.00022507	25	0.00020017	−0.00020291			
37	0.00018969	−0.00019185	36	0.03408838	−0.03496802	36	−0.13847630	0.13972729			
38	0.00060482	−0.00060896	37	0.22889866	−0.23480531	37	0.07282453	−0.07348243			
39	−0.00013151	0.00013416	38	0.11544398	−0.11842298	38	0.06601567	−0.06661205			
40	−0.00037726	0.00037597	39	0.11130147	−0.11417357	39	0.04320074	−0.04359101			
41	0.00000548	−0.00000870	40	0.08655735	−0.08879093	40	0.05713357	−0.05764971			
43	−0.00344607	0.00352173	51	−0.00969200	0.00976482						
44	−0.12187830	0.12455433	52	−0.08930124	0.08997212						
45	−0.02667470	0.02726038	53	−0.02355840	0.02373538						
46	0.10551372	−0.10783044	54	−0.04087515	0.04118223						
47	0.12263501	−0.12532766	55	0.04654853	−0.04689823						
58	0.01461960	−0.01487529									
59	0.01635633	−0.01664239									
60	0.03349750	−0.03408335									
61	−0.03944699	0.04013688									
62	0.05438044	−0.05533152									